

1
2
3
4
5
6
7
8
9
10
11
12
13
14
15
16
17
18
19
20
21
22
23
24
25
26
27
28
29
30
31
32
33
34
35
36
37
38
39

Dynamics of gene expression in single root cells of *A. thaliana*

Ken Jean-Baptiste¹, José L. McFaline-Figueroa¹, Cristina M. Alexandre¹, Michael W. Dorrity^{1,2},
Lauren Saunders¹, Kerry L. Bubb¹, Cole Trapnell¹, Stanley Fields^{1,3}, Christine Queitsch^{1*}, and
Josh T. Cuperus^{1*}

*Corresponding authors: Cuperusj@uw.edu, Queitsch@uw.edu

The author responsible for distribution of materials integral to the findings presented in this article in accordance with the policy described in the Instructions for Authors (www.plantcell.org) is: Josh Cuperus (Cuperusj@uw.edu).

Short title: Single-cell RNA-seq in Arabidopsis roots

1 Department of Genome Sciences, University of Washington, Seattle, WA 98195.

2 Department of Biology, University of Washington, Seattle, WA 98195.

3 Department of Medicine, University of Washington, Seattle, WA 98195.

ABSTRACT

Single-cell RNA-seq can yield high-resolution cell-type-specific expression signatures that reveal new cell types and the developmental trajectories of cell lineages. Here, we apply this approach to *A. thaliana* root cells to capture gene expression in 3,121 root cells. We analyze these data with Monocle 3, which orders single cell transcriptomes in an unsupervised manner and uses machine learning to reconstruct single-cell developmental trajectories along pseudotime. We identify hundreds of genes with cell-type-specific expression, with pseudotime analysis of several cell lineages revealing both known and novel genes that are expressed along a developmental trajectory. We identify transcription factor motifs that are enriched in early and late cells, together with the corresponding candidate transcription factors that likely drive the observed expression patterns. We assess and interpret changes in total RNA expression along developmental trajectories and show that trajectory branch points mark developmental decisions. Finally, by applying heat stress to whole seedlings, we address the longstanding question of possible heterogeneity among cell types in the response to an abiotic stress. Although the response of canonical heat shock genes dominates expression across cell types, subtle but significant differences in other genes can be detected among cell types. Taken together, our results demonstrate that single-cell transcriptomics holds promise for studying plant development and plant physiology with unprecedented resolution.

40

41

42 INTRODUCTION

43 Many features of plant organs such as roots are traceable to specialized cell lineages and their
44 progenitors (Irish, 1991; Petricka et al., 2012). The developmental trajectories of these lineages
45 have been based on tissue-specific and cell-type-specific expression data derived from tissue
46 dissection and reporter gene-enabled cell sorting (Birnbaum et al., 2003; Brady et al., 2007; Li et
47 al., 2016). However, tissue dissection is labor-intensive and imprecise, and cell sorting requires
48 prior knowledge of cell-type-specific promoters and genetic manipulation to generate reporter
49 lines. Few such lines are available for plants other than the reference plant *Arabidopsis thaliana*
50 (Rogers and Benfey, 2015). Advances in single-cell transcriptomics can replace these labor-
51 intensive approaches. Single-cell RNA-seq has been applied to heterogeneous samples of human,
52 worm, and virus origin, among others, yielding an unprecedented depth of cell-type-specific
53 information (Cao et al., 2017; Irish, 1991; Packer and Trapnell, 2018; Russell et al., 2018;
54 Trapnell, 2015; Trapnell et al., 2014).

55

56 While several examples of single cell RNA-seq have been carried out in *Arabidopsis* (Efroni et
57 al., 2016, 2015; Brennecke et al., 2013), they were restricted to only a few cells or cell types. No
58 whole organ single-cell RNA-seq has been attempted in any plant species. The *Arabidopsis*
59 examples focused on root tips, finely dissecting the dynamics of regeneration or assaying
60 technical noise across single cells in a single cell type. Thus, a need exists for larger scale
61 technology that allows a more complete characterization of the dynamics of development across
62 many cell types in an unbiased way. Such technology would increase our ability to assay cell
63 types without reporter gene-enabled cell sorting, identify developmental trajectories, and provide
64 a comparison of how different cell types respond to stresses or drugs. Several high-throughput
65 methods have been described for sequencing of RNA at a high throughput of single cells. Most
66 of these, including most droplet-based methods, rely on the 3' end capture of RNAs. However,
67 unlike with bulk RNA-seq, the data from single cell methods can be sparse, such that genes with
68 low expression can be more difficult to study. Here, we take advantage of expression data from
69 root-specific reporter lines in *A. thaliana* (Birnbaum et al., 2003; Brady et al., 2007; Cartwright
70 et al., 2009; Li et al., 2016) to explore the potential of single-cell RNA-seq to capture the

71 expression of known cell-type-specific genes and to identify new ones. We focus on roots of
72 mature seedlings and probe the developmental trajectories of several cell lineages.

73

74

75 RESULTS

76

77 **Single cell RNA-seq of whole *A. thaliana* roots reveals distinct populations of cortex,** 78 **endodermis, hair, non-hair, and stele cells**

79 We used whole *A. thaliana* roots from seven-day-old seedlings to generate protoplasts for
80 transcriptome analysis using the 10x Genomics platform (**Supplemental Figure 1A**). We
81 captured 3,121 root cells to obtain a median of 6,152 unique molecular identifiers (UMIs) per
82 cell. UMIs here are 10 base random tags added to the cDNA molecules that allow us to
83 differentiate unique cDNAs from PCR duplicates. These UMIs corresponded to the expression of
84 a median of 2,445 genes per cell and a total of 22,419 genes, close to the gene content of *A.*
85 *thaliana*. Quality measures for sequencing and read mapping were high. Of the approximately
86 79,483,000 reads, 73.5% mapped to the TAIR10 *A. thaliana* genome assembly, with 67% of
87 these annotated transcripts. These values are well within the range reported for droplet-based
88 single-cell RNA-seq in animals and humans.

89

90 For data analysis, we applied Monocle 3, which orders transcriptome profiles of single cells in an
91 unsupervised manner without *a priori* knowledge of marker genes (Qiu et al., 2017a; Qiu et al.,
92 2017b; Trapnell et al., 2014). We used the 1500 genes in the data set (**Supplemental Data Set 1**)
93 that showed the highest variation in expression (**Supplemental Figure 1B**). For unsupervised
94 clustering, we used 25 principal components (PC). These 25 PCs accounted for 72.5% of the
95 variance explained by the first 100 PCs, with the first PC explaining 11% and the 25th PC
96 explaining 0.9% (**Supplemental Figure 1C**). Cells were projected onto two dimensions using
97 the uniform manifold approximation and projection (UMAP) method (McInnes and Healy, 2018)
98 and clustered, resulting in 11 clusters (**Figure 1A**) (Blondel et al., 2008). Most clusters showed
99 similar levels of total nuclear mRNA, although clusters 9 and 11 were exceptions with higher
100 levels (**Supplemental Figure 1D**). Because some of the UMAP clusters, specifically clusters 9
101 and 11, consisted of cells that had higher than average amounts of nuclear mRNA, we were
102 concerned that these clusters consisted merely of cells that were doublets, *i.e.* two (or more) cells
103 that received the same barcode and that resulted in a hybrid transcriptome. As cells were
104 physically separated by digestion, it was possible that two cells remained partially attached. In
105 order to identify potential doublets in our data, we performed a doublet analysis using Scrublet

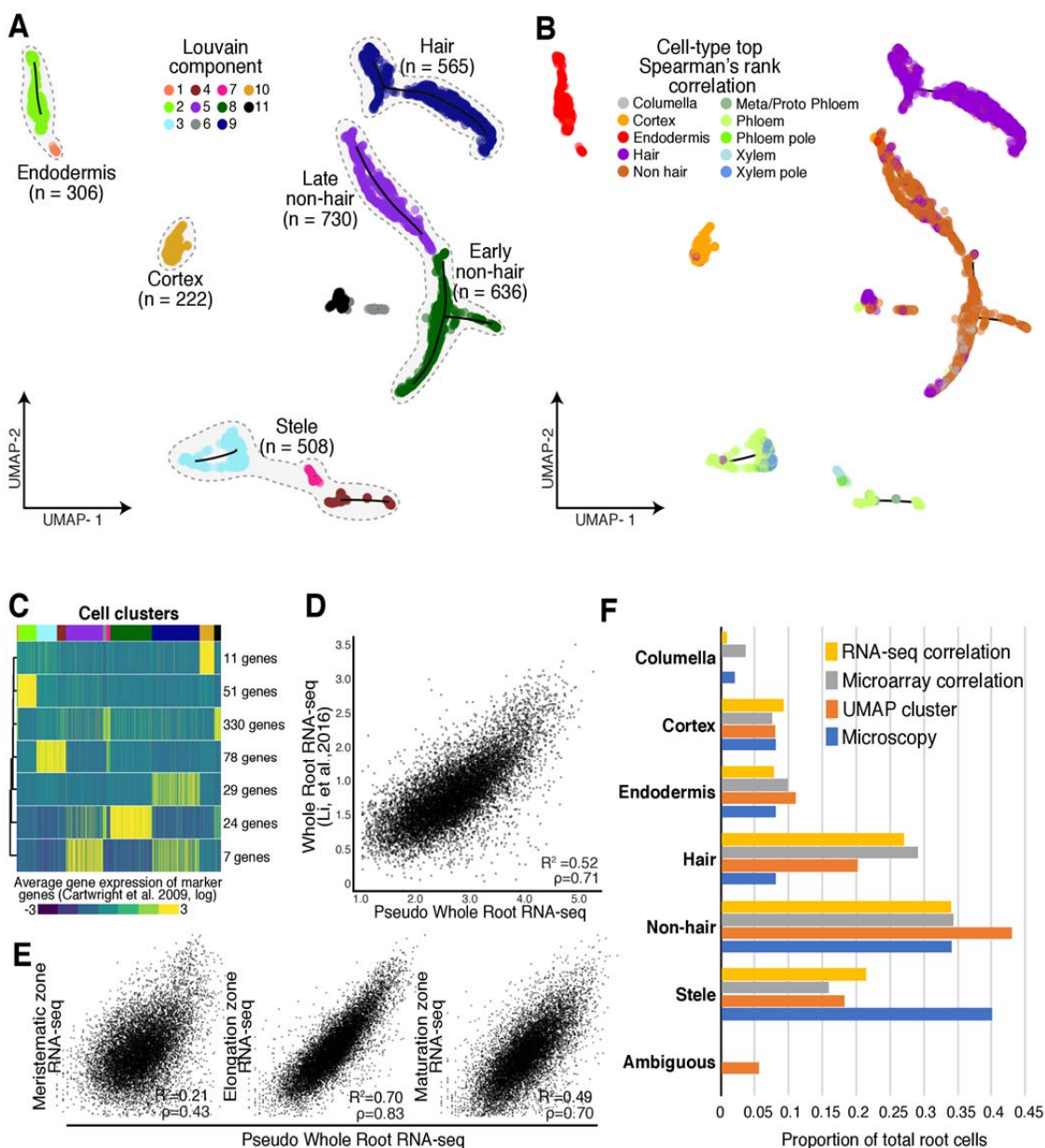


Figure 1. Annotation of cell and tissue types for single-cell RNA-seq of whole *A. thaliana* roots.

(A) Root cells were clustered and projected onto two-dimensional space with UMAP (McInnes and Healy, 2018). Filled circles represent individual cells; colors represent their respective Louvain component. Monocle 3 trajectories (black lines) are shown for clusters in which a trajectory could be identified. (B) Filled circles represent individual cells; colors indicate cell and tissue type based on highest Spearman's rank correlation with sorted tissue-specific bulk expression data (Brady et al., 2007; Cartwright et al., 2009). (C) Known marker genes (Brady et al., 2007; Cartwright et al., 2009) were used to cluster single-cell gene expression profiles based on similarity. The expression of 530 known marker genes was grouped into 7 clusters, using k-means clustering. Mean expression for each cluster (rows) is presented for each cell (columns). Cells were ordered by their respective Louvain component indicated above by color (see A, starting at component 1 at left). Number of genes in each cluster is denoted at right. (D) Single-cell RNA-seq pseudo-bulked expression data are compared to bulk expression data of whole roots (Li et al., 2016). (E) Single-cell pseudo-bulk expression data are compared to bulk-expression data of the three developmental regions of the *A. thaliana* root (Li et al., 2016). (F) Proportions of cells as annotated by either UMAP (in A), Spearman's rank correlation (in B), or Pearson's rank correlation (in Supplemental Figure 2), are compared to proportions determined by microscopy (Brady et al., 2007; Cartwright et al., 2009).

106 (Wolock et al., 2018), which uses barcode and UMI information to calculate the probability that

107 a cell is a doublet. This analysis identified only 6 cells, of 3,021 cells analyzed, as doublets,
108 spread across multiple UMAP clusters and multiple cell types (**Supplemental Figure 1E**).
109 Overall, given the low number of doublets, we did not attempt to remove these cells.

110
111 To assign these clusters to cell types, we performed three complementary analyses relying on
112 two expression data sets from tissue-specific and cell-type-specific reporter lines: an earlier one
113 generated with microarrays (Brady et al., 2007; Cartwright et al., 2009) and a more recent one
114 generated with RNA-seq and a greater number of lines (Li et al., 2016). We first compared the
115 microarray expression data for each reporter line to the gene expression values in each single
116 cell, using Spearman's rank correlations to assign each cell a cell type identity based on highest
117 correlation of gene expression (**Figure 1B, Supplemental Data Set 2**) (Brady et al., 2007;
118 Cartwright et al., 2009). Second, we compared the RNA-seq expression data to the gene
119 expression values in each single cell by Pearson's correlation (Li et al., 2016, **Supplemental**
120 **Figure 2A**). Third, we examined the expression of 530 cell-type-specific marker genes (Brady et
121 al., 2007) by defining seven marker gene clusters with k-means clustering and calculating their
122 average expression for each cell. We then compared each cell's UMAP Louvain component
123 cluster assignment (**Figure 1A**) with its marker-gene-based assignment. Louvain components
124 were derived using the Louvain method for community detection (Blondel et al., 2008) which is
125 implemented in Monocle 3. Unlike k-means clustering for which the user provides the desired
126 number of clusters to partition a dataset, Louvain clustering optimizes modularity (*i.e.* the
127 separation of clusters based on similarity within a cluster and among clusters), aiming for high
128 density of cells within a cluster compared to sparse density for cells belonging to different
129 clusters. The 11 clusters presented in **Figure 1A** optimized the modularity of the generated
130 expression data and were not defined by us.

131
132 In general, the UMAP clusters showed high and cluster-specific expression of marker genes. For
133 example, cells in cluster 10 showed high and specific mean expression of cortex marker genes
134 (**Figure 1C, Supplemental Figure 3, Supplemental Data Set 3**). Both expression correlations
135 and marker gene expression allowed us to assign the Louvain components to five major groups:
136 root hair cells, non-hair cells (containing both an early and late cluster), cortex cells, endodermis
137 cells and stele cells (containing both xylem and phloem cells) (**Figure 1A**). Although some cells

138 were most highly correlated in expression with the cell type columella in Spearman's rank tests
139 and RNA-seq Pearson's correlation, these cells co-clustered with non-hair cells (**Figure 1B,**
140 **Supplemental Figure 2**). This finding is consistent with bulk RNA-seq data of sorted cells (Li et
141 al., 2016). Specifically, the *PET11* (columella) -sorted bulk RNA-seq data are most similar to
142 bulk RNA-seq data sorted for *GL2* and *WER* (Li et al., 2016), both of which mark non-hair cells
143 (Petricka et al., 2012). Therefore, these cells were grouped as early non-hair cells with other non-
144 hair cells in Louvain component 8. As their expression values were best correlated with RNA-
145 seq data for *WER*-sorted cells, they likely represent a mix of early non-hair and lateral root cap
146 cells, which have very similar expression profiles (**Supplemental Figure 2**).

147
148 We assessed the extent to which combined single-cell root expression data resembled bulk whole
149 root expression data (Li et al., 2016) (**Figure 1D, E**). We observed strong correlations between
150 these two data sets (Pearson's correlation coefficient [R^2]=0.52, Spearman's ρ =0.71). We also
151 compared the combined single-cell expression data to three bulk expression data sets
152 representing the major developmental zones in the *A. thaliana* root: the meristematic zone, the
153 elongation zone, and the maturation zone (**Figure 1E**). We observed the highest correlation of
154 single-cell and bulk expression in the elongation zone (R^2 =0.70, ρ =0.83) and a lower correlation
155 in the maturation zone (R^2 =0.58, ρ =0.70). This observation is surprising given the more mature
156 developmental stage of the harvested roots (**Supplemental Figure 1A**), and likely reflects that
157 younger cells are more easily digested during protoplasting and contribute in greater numbers to
158 the gene expression data. As expected, single-cell and bulk expression were poorly correlated in
159 the meristematic zone (R^2 =0.11, ρ =0.43), as meristematic tissue accounts for only a small
160 proportion of mature roots. Furthermore, we compared tissue-specific expression (Li et al., 2016)
161 to expression both in the annotated cell clusters and in cells expressing appropriate marker genes.
162 In general, we found strong correlations among these data sets, suggesting that the clusters are
163 annotated correctly (**Supplemental Table 1**).

164
165 We also compared the relative representation of root cell types between our data set and
166 estimates based on microscopy studies (**Figure 1F**) (Brady et al., 2007; Cartwright et al., 2009).
167 Independent of annotation method, we observed the expected numbers of cortex (222
168 Spearman's/ 233 UMAP), endodermis (306/ 304), non-hair cells (1201/ 1061) and columella

169 cells (111/ no UMAP cluster). Hair cells (565/ 898) were overrepresented whereas stele cells
170 (508/ 490) were underrepresented, possibly reflecting a bias in the protoplast preparation of
171 whole root tissue.

172
173 Protoplasting, the removal of the plant cell wall, alters the expression of 346 genes (Birnbaum et
174 al., 2003); 76 of these genes were included in the 1500 genes with the highest variation in
175 expression (**Supplemental Data Set 1, Supplemental Figure 1B**) that we used for clustering.
176 Some of the 76 genes showed cell-type-specific expression. To exclude the possibility that the
177 expression pattern of these genes produced artefactual clusters and cell-type annotations, we
178 removed them from the analysis and re-clustered, which resulted in a similar UMAP
179 visualization, with similar numbers of Louvain components and cell types.

180

181 **Single-cell RNA-seq of identifies novel genes with cell-type and tissue-type-specific** 182 **expression**

183 Some marker genes are not expressed exclusively in a single cell type, making it desirable to
184 identify additional genes with cell-type-specific expression. We first confirmed the high and
185 cluster-specific expression of well-known marker genes (**Figure 2A, Supplemental Figure 4**)
186 (Li et al., 2016) such as the root-hair-specific *COBL9*, the endodermis-specific *SCR* and the three
187 stele-specific genes *MYB46* (xylem-specific), *APL* (phloem-specific), and *SUC2* (phloem-
188 specific). The nonspecific expression of the quiescent center cell marker genes *WOX5* and
189 *AGL42* is likely due to the failure to capture sufficient numbers of these rare cells. The
190 nonspecific expression of *WOL* and the more heterogeneous pattern of both *WER* and *GL2*
191 expression have been previously observed (Brady et al., 2007; Winter et al., 2007).

192 Second, to find novel marker genes, we identified genes with significantly different expression
193 within and among Louvain component clusters by applying the Moran's I test implemented in
194 Monocle 3. We found 317 genes with cluster-specific expression, 164 of which were novel,
195 including at least one in each cluster (**Figure 2A, Supplemental Data Set 4**). Using cell-type
196 annotations rather than Louvain clusters, we identified 510 genes with cell-type-specific
197 expression, of which 317 overlapped with the Louvain component cluster-specific expression
198 genes, as well as an additional 125 novel genes, some of which have been implicated in the
199 development of a cell lineage in targeted molecular genetics studies.

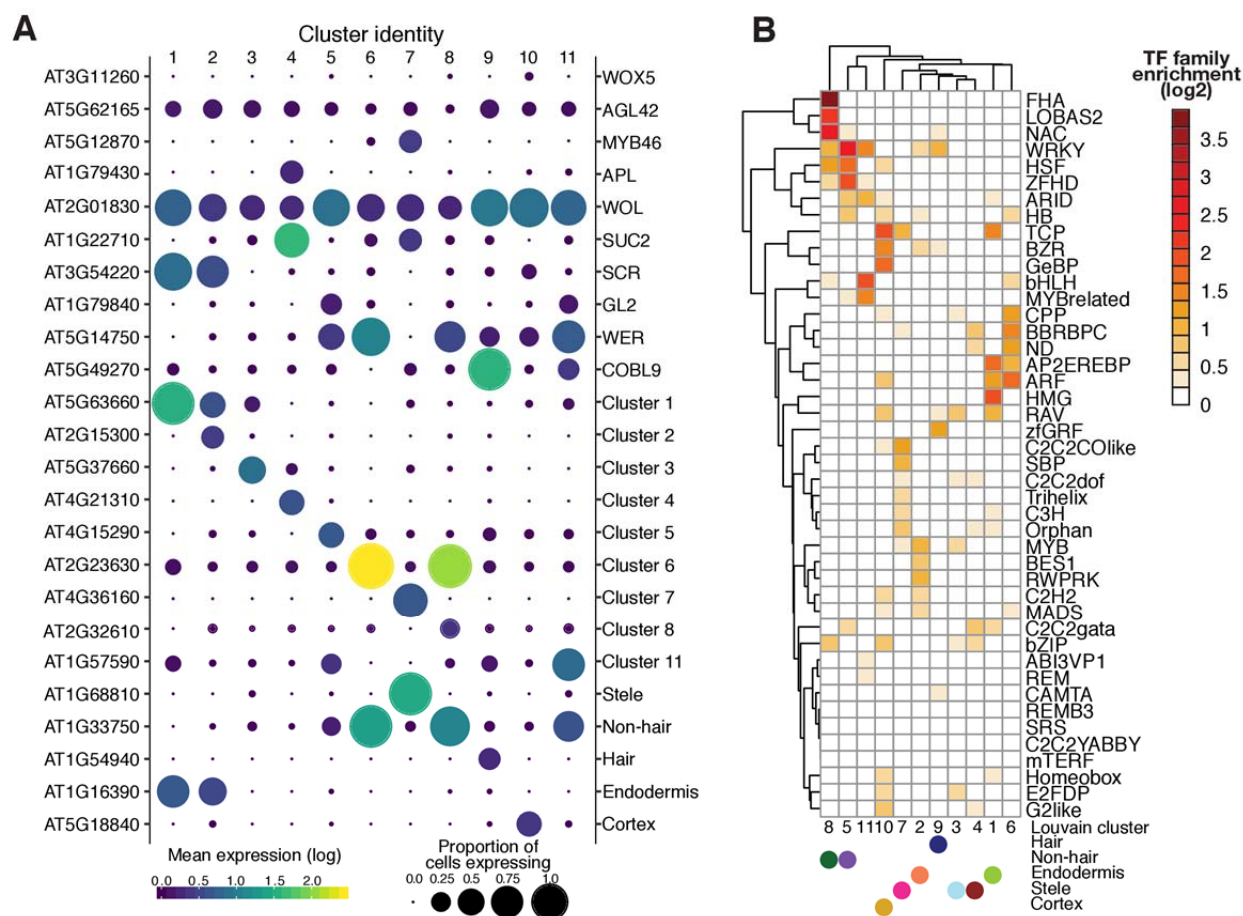


Figure 2. Novel cluster-specific and tissue-specific genes and enriched transcription factor motifs.

(A) Proportion of cells (circle size) and mean expression (circle color) of genes with cluster-specific and tissue-specific expression are shown, beginning with known marker genes labeled with their common name (right) and their systematic name (left). For novel genes, the top significant cluster-specific genes are shown, followed by the top significant tissue-specific genes; both were identified by principal graph tests (Moran's I) as implemented in Monocle 3. Note the correspondence between Louvain components and cell and tissue types. For all novel cluster-specific and tissue-specific genes, see Supplemental Table 3. **(B)** Enrichments of known transcription factor motifs (O'Malley et al., 2016) 500 bp upstream of genes with cluster-specific expression compared to genome background. Motifs are specific to transcription factor gene families rather than individual genes. The plot is clustered based on similarity in enrichments with Louvain components and cell and tissue types (filled circles) indicated.

200
201 For example, the stele-specific AT1G8810 (*ABS5*, *T5LI*) gene (cluster 7, **Figure 2A**) encodes a
202 bHLH protein that promotes vascular cell division and differentiation as part of a heterodimer
203 with second bHLH protein, LHW (Katayama et al., 2015; Ohashi-Ito et al., 2014). Another stele-
204 specific gene, AT4G36160 (*ANAC076*, *VND2*) (cluster 7), encodes a ClassIIB NAC-domain
205 transcription factor that contributes to xylem vessel element differentiation by promoting
206 secondary cell wall formation and programmed cell death (Tan et al., 2018). In tissue-specific
207 bulk data (Brady et al., 2007; Winter et al., 2007), both genes show xylem-specific expression

208 consistent with their biological functions; *T5LI* expression is high only in the meristematic and
209 elongation zones, while *VND2* expression starts in the elongation zone and persists throughout
210 the maturation zone. Other genes, not previously implicated in root development, show tissue-
211 specific bulk expression patterns consistent with the single-cell data. For example, AT1G54940
212 (*GUX4*, *PGSIP4*), which encodes a xylan glucuronosyltransferase (Lee et al., 2012; Mortimer et
213 al., 2010), was specifically expressed in hair cells (cluster 9) and is most highly expressed in
214 cells destined to become hair cells in the elongation zone and in differentiated hair cells in the
215 maturation zone (Brady et al., 2007; Cartwright et al., 2009).

216

217 **Expression of some transcription factors shows high correlation with specific cell types**

218 We asked whether we could identify transcription factors that may contribute to the cluster-
219 specific expression patterns. To do so, we tested for transcription factor motif enrichments in the
220 proximal regulatory regions of genes with cluster-specific expression, examining 500 bp
221 upstream of the transcription start site (Alexandre et al., 2018; Sullivan et al., 2014) and a
222 comprehensive collection of *A. thaliana* transcription factor motifs (O'Malley et al., 2016). This
223 analysis revealed significant transcription factor motif enrichments among clusters and annotated
224 major tissues and cell types (**Figure 2B**).

225

226 As transcription factors in *A. thaliana* often belong to large gene families without factor-specific
227 motif information (Riechmann et al., 2000), it is challenging to deduce the identity of the specific
228 transcription factor that drives cluster-specific transcription factor motif enrichment and
229 expression. As an approximation, we examined transcription factors that were expressed in the
230 cluster or tissue in which a significant enrichment of their motif was found, or in neighboring
231 cell layers (some factors move between cells (Petricka et al., 2012)) (**Supplemental Data Set 4**).
232 We focused first on the small *BZR/BEH* gene family whose motif was specifically enriched in
233 cortex cells (cluster 10). Of the six genes (BEH1/AT3G50750, BEH2/AT4G36780,
234 BEH3/AT4G18890, BEH4/AT1G78700, BES1/AT1G19350, and BZR1/AT1G75080) the single
235 recessive *beh4*, *bes1*, and *bzr1* mutants exhibit altered hypocotyl length (Lachowiec et al., 2018).
236 Double mutant analysis suggests partial functional redundancy, which agrees with our
237 observation of overlapping expression patterns for these genes across cell types (**Supplemental**
238 **Figure 5A, B**). In contrast, neither *beh1* and *beh2* single mutants nor the respective double

239 mutant show phenotypic defects (Lachowiec et al., 2018). However, *BEH2* was the most highly
240 expressed *BZR/BEH* family member across clusters and annotated root tissue and cell types
241 (**Supplemental Figure 5A, B**). Although *BEH4*, the most ancient family member with the
242 strongest phenotypic impact, showed cortex-specific expression, none of the *BZR/BEH* genes
243 showed significance for cluster-specific expression, suggesting that combinations of family
244 members, possibly as heterodimers, may result in the corresponding motif enrichment in cortex
245 cells (**Supplemental Figure 5A, B**). In particular, *BES1* and *BZR* expression was highly
246 correlated, consistent with these genes being the most recent duplicates in the family
247 (**Supplemental Figure 5C**) (Lachowiec et al., 2013; Lan and Pritchard, 2016).

248
249 In contrast to the *BEH/BZR* gene family, we found stronger cluster specificity for some TCP
250 transcription factors. The TCP motif was strongly enriched in cortex (cluster 10), endodermis
251 (cluster 1) and stele (cluster 7). Of the 24 TCP transcription factors, we detected expression for
252 eight. Of these, *TCP14* (AT3G47620) and *TCP15* (AT1G69690) were expressed primarily in
253 stele (clusters 7 and 4) although this cluster-specific expression was not statistically significant
254 (**Figure 2B, Supplemental Figure 5D, E, Supplemental Data Set 4**). *TCP14* and *TCP15* are
255 class I TCP factors thought to promote development. Acting together, *TCP14* and *TCP15*
256 promote cell division in young internodes (Kieffer et al., 2011), seed germination (Resentini et
257 al., 2015), cytokinin and auxin responses during gynoecium development (Lucero et al., 2015),
258 and repression of endoreduplication (Peng et al., 2015). Both genes are expressed in stele in bulk
259 tissue data (Brady et al., 2007; Winter et al., 2007), with *TCP14* expression also observed in the
260 vasculature by *in situ* hybridization (Tatematsu et al., 2008). *TCP14* can affect gene expression
261 in a non-cell-autonomous manner.

262
263 To further investigate the co-occurrence of cluster-specific transcription factor motif enrichments
264 with transcription factor expression, we next examined the novel genes with significant cluster-
265 specific expression. Eight of these encode transcription factors with corresponding highly
266 enriched cluster-specific binding motifs. For one of these, *BRN2* (AT4G10350), cluster-specific
267 expression coincided with enrichment of the NAC transcription factor family motif (cluster 8,
268 non-hair and lateral root cap cells, **Figure 2B**). *BRN2* encodes a ClassIIB NAC transcription
269 factor implicated in root cap maturation together with *BRN1* and *SMB*. Class IIB NAC

270 transcription factors are thought to contribute to terminal cell differentiation accompanied by
271 strong cell wall modifications (Bennett et al., 2010). In our data, *BRN2* was most highly
272 expressed in cluster 8 (non-hair and lateral root cap cells) and less so in cluster 6 (**Supplemental**
273 **Data Set 4**).

274

275 **Clustering stele cells identifies novel genes with cell-type specific expression in the** 276 **vasculature**

277 Our initial attempts to annotate and separate cell types within stele tissue with marker gene
278 expression or Spearman's rank correlations failed. Instead, we separately clustered stele cells to
279 reveal 6 sub-clusters upon UMAP visualization, with 5 sub-clusters containing more than 40
280 cells. Their annotation via Spearman's rank correlation with sorted bulk data was not successful;
281 however, using well-established marker genes expression, we detected cluster-specific
282 expression patterns (**Figure 3A and B**).

283

284 Cells closely related to xylem pole pericycle constituted the largest group of cells (205 cells);
285 phloem pole pericycle cells were the second largest (84 cells). The high number of pericycle
286 cells likely reflects our experimental procedure, as these cells reside on the exterior of the
287 vascular bundle. Both phloem and xylem clusters showed similar numbers of cells (77 cells and
288 72 cells respectively); the phloem companion cells formed a distinct cluster. We observed the
289 expected sub-cluster expression for several known genes and marker genes and identified novel
290 genes with sub-cluster-specific expression (**Figure 3C, D, Supplemental Data Set 1**). Although
291 there was some discrepancy, especially for the *APL* gene, which is expressed in both companion
292 and phloem cells (**Figure 3C**), this is largely due to missing data.

293

294 **Pseudotime trajectories coincide with the development stages of cortex, endodermis, and** 295 **hair cells**

296 We next sought to visualize the continuous program of gene expression changes that occurs as
297 each cell type in root differentiates. Because whole roots contain a mix of cells at varying
298 developmental stages, we reasoned that our experiment should have captured a representative
299 snapshot of their differentiation. Monocle not only clusters cells by type but also places them in
300 "pseudotime" order along a trajectory that describes their maturity. To make these trajectories,

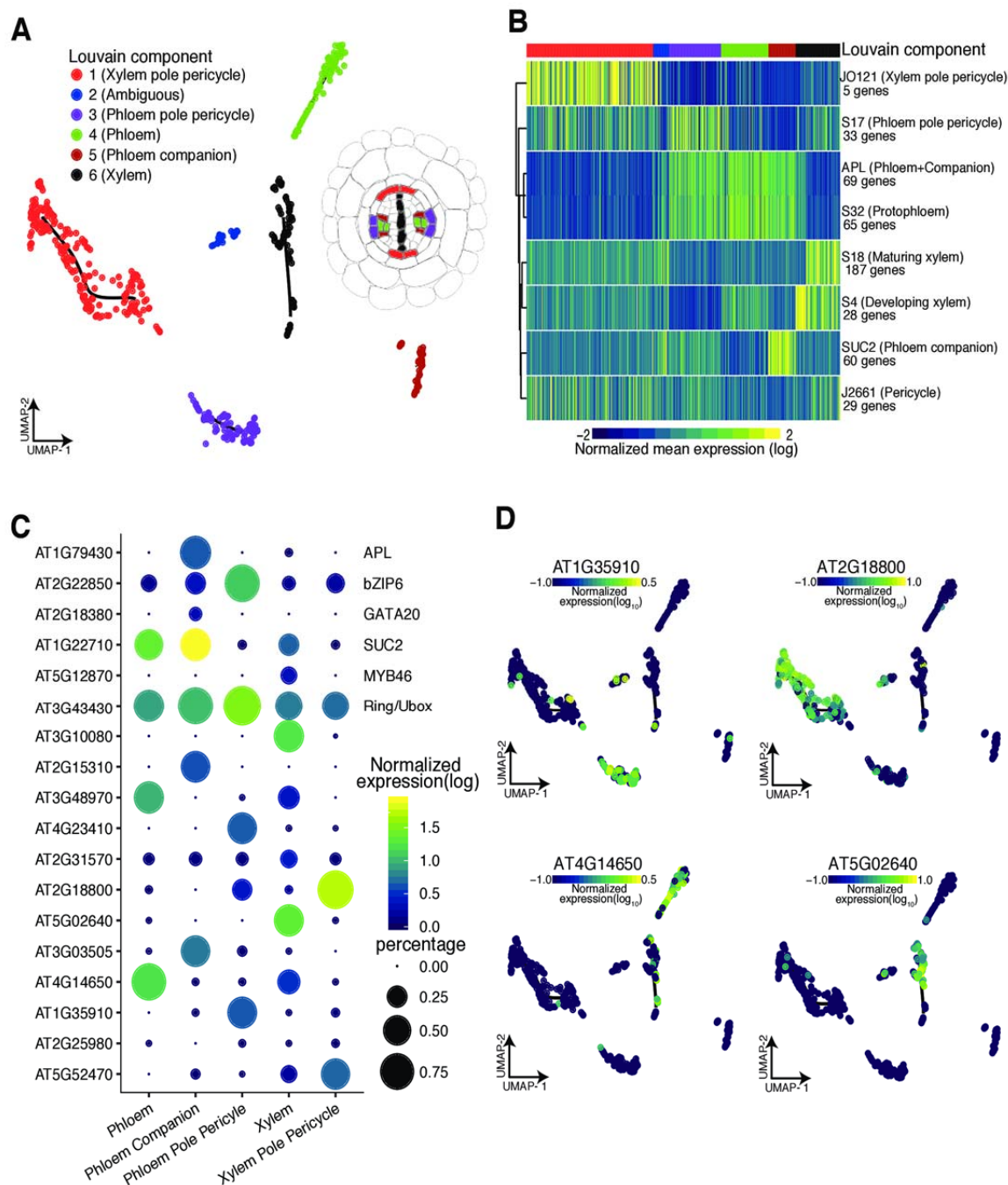


Figure 3. Re-clustering of stele cells yields distinct sub-clusters of vasculature cell types.

(A) Cells initially annotated as stele tissue were re-clustered, resulting in six distinct sub-clusters cells, five of which contained more than 40 cells. (B) Mean expression for previously identified cell-type specific genes (Cartwright et al., 2009) in each cell is shown, allowing annotation of stele sub-cluster identities as shown in (A). (C) Proportion of cells (circle size) and mean expression (circle color) of genes with cluster-specific and tissue-specific expression are shown, starting with known marker genes at the top, labeled with their common name (right) and their systematic name (left). Below, novel significant tissue-specific genes are shown with their systematic names, identified by principal graph tests (Moran's I) as implemented in Monocle 3. (D) Example expression overlays for cluster-specific genes identified by the principal graph test in (C).

301 Monocle 3 learns an explicit principal graph from the single-cell-expression data through

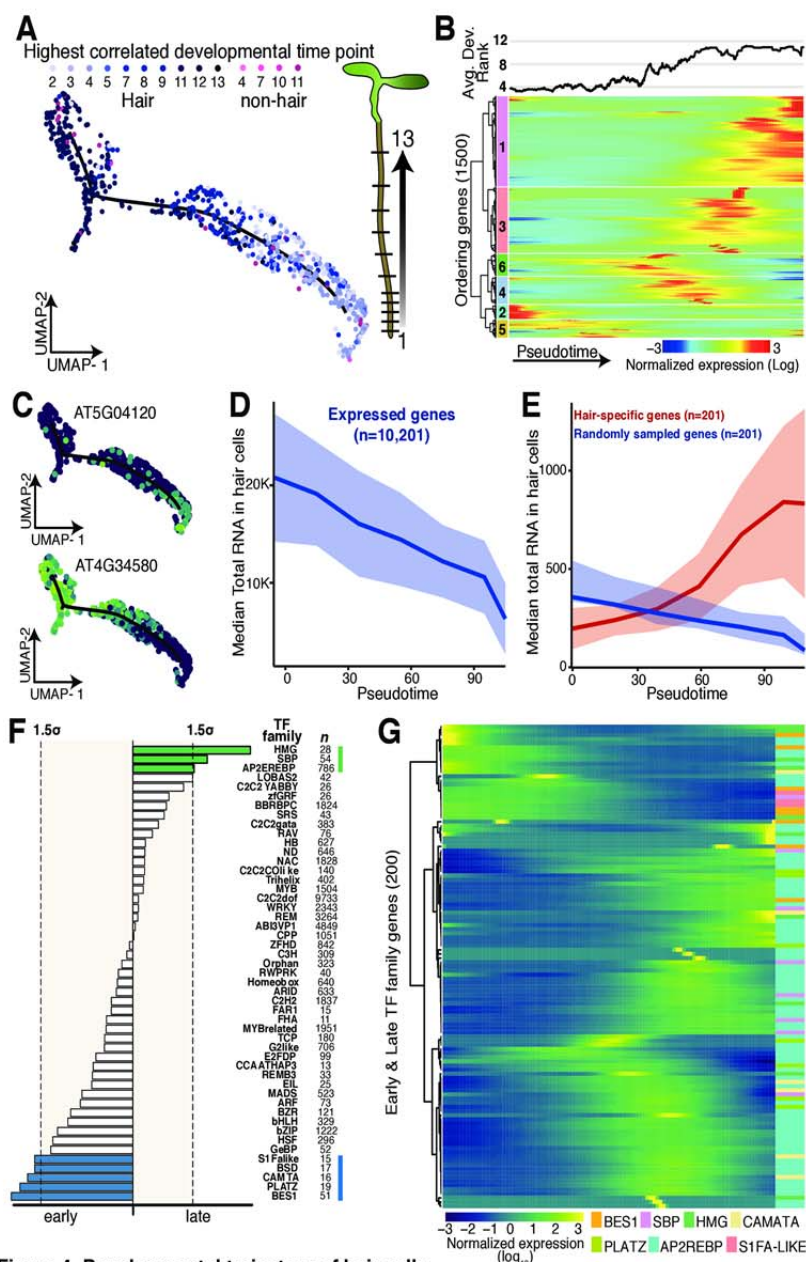


Figure 4. Developmental trajectory of hair cells.

(A) UMAP-clustered hair cells were assigned a developmental time point based on highest Spearman's rank correlation with bulk expression data of staged tissue (13 developmental stages) (Brady et al., 2007; Cartwright et al., 2009). Cell type and developmental time points are indicated in shades of blue (and pink). Graphic illustrates developmental stages in *A. thaliana* root (Plant Illustrations). (B) Cells were ordered in pseudotime; columns represent cells, rows represent expression of the 1500 ordering genes. Rows were grouped based on similarity in gene expression, resulting in 6 clusters (indicated left), with genes in clusters 2 and 5 expressed early in pseudotime and genes in cluster 1 expressed late. Hair cells with the earliest developmental signal (Brady et al., 2007; Cartwright et al., 2009) were designated as the root of the trajectory. The graph above represents the average best-correlation of developmental stage (Brady et al., 2007; Cartwright et al., 2009) in a scrolling window of 20 cells with pseudotime, showing the expected increase in developmental age with increasing pseudotime. (C) Examples of an early and a late expressed hair-cell-specific gene. Gene expression in each cell is superimposed onto the UMAP cluster and trajectory, with lighter colors indicating higher gene expression. (D) Median total RNA captured in cells decreases across pseudotime. Number of genes included is indicated. (E) Comparison of median total RNA for hair-cell-specific genes (in red) to a comparable random set of genes (in blue). Number of genes is indicated (Permutation test p-value $\approx 1 \times 10^{-4}$). (F) Different transcription factor motifs reside in the 500 bp upstream regions of genes expressed early (clusters 2, 5) compared to genes expressed late (cluster 1). Transcription factor motifs specific to early hair cells are denoted with blue bars, those for late hair cells with green bars; bar length indicates motif frequency. Thresholds on either side (grey box, dotted lines) refer to 1.5 standard deviation above mean motif frequency. (G) Expression of individual members of transcription factors families highlighted in D across pseudotime identifies candidate factors driving early or late gene expression.

2017b; Trapnell et al., 2014). To dissect the developmental dynamics of individual clusters, we first focused on the well-defined root-hair cells, in which combined single-cell expression values highly correlated with those from bulk protoplasts sorted for expression of the *COBL9* root-hair marker gene (**Supplemental Table 1**). To annotate the unsupervised trajectory that Monocle 3 created for hair cells, we used the Spearman's rank test to compare expression in all cells to bulk expression data representing 13 different developmental stages in root tissues from all the available sorted cell types (**Supplemental Figure 6**) (Brady et al., 2007; Cartwright et al., 2009). Each cell was assigned the developmental stage and cell type most correlated with its expression values (**Figure 4A**). The hair cells with the earliest developmental stage assignment were designated as the root of the trajectory. Next, pseudotime was calculated for all other hair cells based on their distance from the root of the trajectory (**Figure 4B**). We compared this calculated pseudotime with the most highly correlated developmental assignment from bulk data, finding close agreement (**Figure 4B**). Examples of genes that are expressed early and late in pseudotime in the UMAP hair cluster are shown in **Figure 4C**.

Hair cells undergo endoreduplication as they mature, resulting in up to 16N genomic copies in the developmental stages assayed (Bhosale et al., 2018). Although endoreduplication is thought to increase transcription rates (Bourdon et al., 2012), general transcription might decrease as hair-cell-specific genes become more highly expressed during hair cell differentiation. Single-cell RNA-seq affords us the opportunity to explore whether transcription rates differ across development. Single-cell RNA-seq can measure both relative expression (as in bulk RNA-seq) and the total number of RNA molecules per cell. The total amount of cellular mRNA was drastically reduced across hair cell development (**Figure 4D**). This result may be due to technical bias; for example, gene expression in larger, endoreduplicated cells may be more difficult to assess with this droplet-based method. If so, the observed reduction in captured transcripts should affect all genes more or less equally. Alternatively, this observation may reflect hair cell differentiation, whereby transcription of hair-cell-specific genes should remain unaffected or increase over pseudotime. Our results support the latter scenario as transcription of hair-cell-specific genes appears to increase over pseudotime, consistent with these cells undergoing differentiation towards terminally differentiated hair cells (**Figure 4E, Supplemental Figure 7A**).

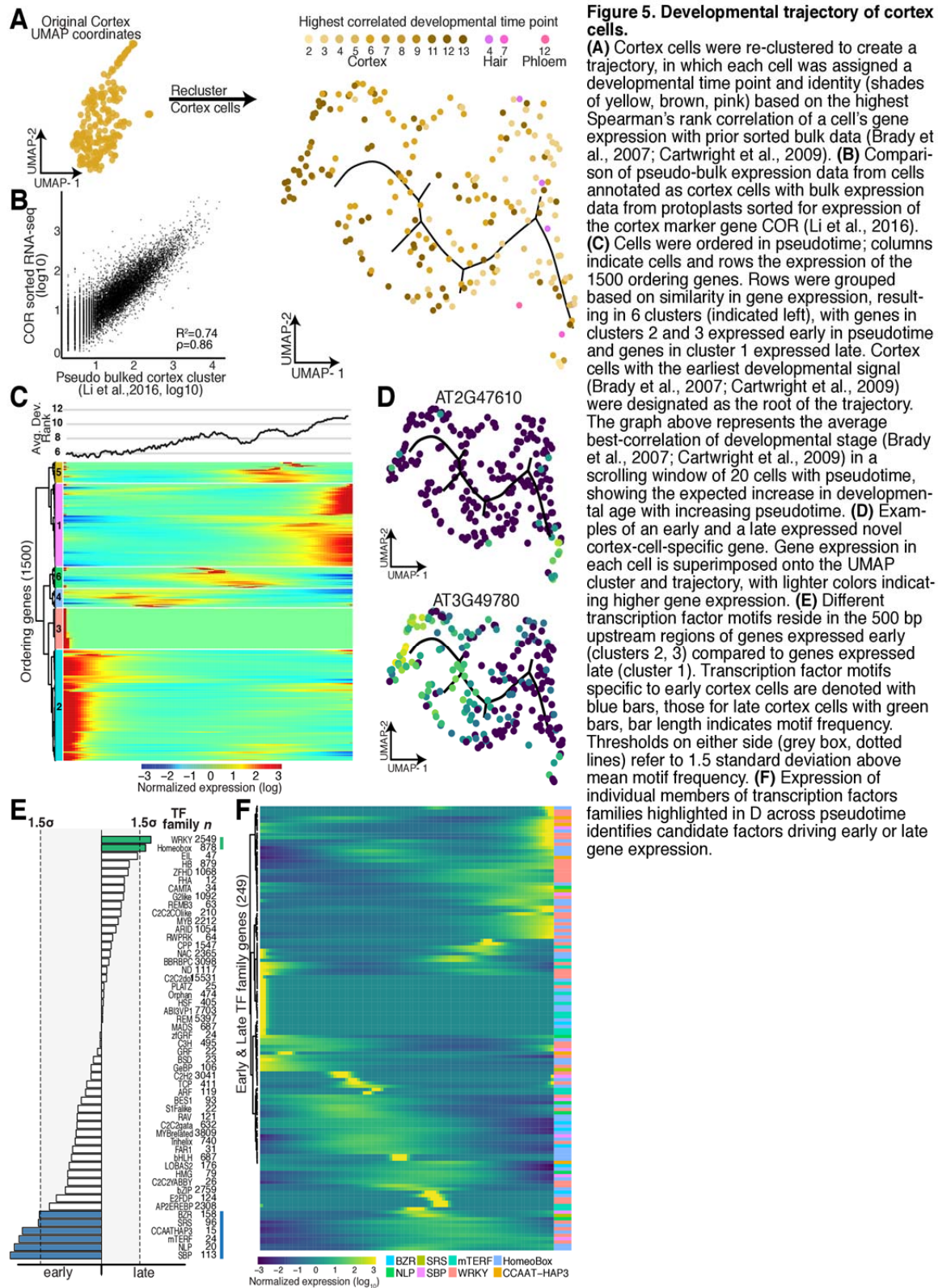
334

335 To further explore this transcriptional dynamic, we calculated RNA velocity (La Manno et al.,
336 2018), a measure of the transcriptional rate of each gene in each cell of the hair cell cluster. RNA
337 velocity takes advantage of errors in priming during 3' end reverse transcription to determine the
338 splicing rate per gene and cell. It compares nascent (unspliced) mRNA to mature (spliced)
339 mRNA; an overall relative higher ratio of unspliced to spliced transcripts indicates that
340 transcription is increasing. In our data, only ~4% of reads were informative for annotating
341 splicing rates, a lower percentage than what has been used in mammalian cells for velocity
342 analyses, and thus our results may be less reliable. Based on data for 996 genes, mean RNA
343 velocity increased across pseudotime (**Supplemental Figure 7B**, $p = 2.2 \times 10^{-16}$ linear model, $\rho = 0.73$). This increase in velocity was associated with the predicted changes in endoreduplication
344 (Bhosale et al., 2018), especially between the 4N and 8N stages (**Supplemental Figure 7C**,
345 Tukey's multiple comparison p -value = 0.0477).

347

348 We also observed developmental signals in other cell types, including cortex and endodermis
349 (**Figure 5A-D, Supplemental Figure 8**). Combined single-cell expression values for cortex cells
350 highly correlated with those from bulk protoplasts sorted for expression of the *COR* cortex
351 marker gene (**Figure 5B**, $R^2 = 0.74$, $\rho = 0.86$). As Monocle 3 did not identify a trajectory for
352 cortex cells in the context of all cells, we isolated the cortex cells and re-performed UMAP
353 dimensionality reduction, clustering, and graph embedding (**Supplemental Data Set 1**). Each
354 cortex cell was assigned a developmental stage based on its Spearman's rank correlation with
355 bulk expression data (Brady et al., 2007; Cartwright et al., 2009). Cortex cells with the earliest
356 developmental signal were designated as the root of the cortex trajectory, and pseudotime was
357 assigned to the remaining cortex cells based on their distance from the root (**Figure 5A-D**,
358 **Supplemental Figure 6**). As pseudotime increased for cortex cells, so did their age, indicating
359 good agreement of the trajectory with developmental bulk RNA-seq data. Although we observed
360 some decrease in total RNA expression and increased expression in cell-type specific genes for
361 endodermis, we did not see a clear pattern of change in total RNA across cortex pseudotime
362 (**Supplemental Figures 8 & 9**).

363



364 We asked whether we could assign the transcription factors that drive gene expression along

365 these developmental trajectories in early and late hair, cortex, and endodermis cells. As before,
366 we first analyzed transcription factor motif enrichments and then explored the expression of the
367 corresponding transcription factor gene families. Indeed, for most developmentally enriched
368 transcription factor motifs, we could pinpoint candidate transcription factors that are expressed
369 either early or late. For example, the *AP2/EREBP* (APETALA2/ethylene responsive element
370 binding protein) transcription factor family is one of the largest in *A. thaliana* (Riechmann et al.,
371 2000), with nearly 80 covered in our data set; of these, only four (AT2G25820, At5G65130,
372 AT1G36060, AT1G44830) showed strong expression in late hair cells (**Figure 4F, G,**
373 **Supplemental Figure 10**). One of these, AT1G36060 (Translucent Green), regulates expression
374 of aquaporin genes (Zhu et al., 2014). Overexpression of this gene confers greater drought
375 tolerance (Zhu et al., 2014), consistent with its expression in older hair cells. Similar examples of
376 developmental stage-specific motif enrichments with corresponding transcription factor
377 expression were also found for cortex and endodermis (**Figure 5E, F, Supplemental Figure 8,**
378 **Supplemental Figure 10**).

379

380 **Branch points in developmental trajectories mark developmental decisions**

381 Although a developmental trajectory that reflects the differentiation from early to late cells
382 within a cell type should be branchless, we did observe some branch points, for example in
383 Louvain component 8, affording us the opportunity to explore their biological relevance. As
384 discussed, Louvain component 8 contains early non-hair cells and likely some lateral root cap
385 cells. To further explore the cells within the branch, we performed a principal graph test,
386 comparing their expression profiles to those of cells elsewhere in the cluster (**Figure 6A**). We
387 found that cells within the branch were significantly enriched for expression of genes involved in
388 cell plate formation, cytokinesis and cell cycle. We explored this enrichment for cell cycle
389 annotations by comparing expression of previously identified core cell cycle genes (Gutierrez,
390 2009) in cells within the branch to cells in the rest of the cluster, finding many core cell cycle
391 genes, in particular many G2 genes, to be specifically expressed in branch cells (**Figure 6B**).
392 Among these genes were several of the cyclin-dependent kinase B family members that direct
393 the G2 to M transition. Two cyclin-dependent kinase subunits (*CKS1* and *CKS2*), thought to
394 interact with several *CDK* family members, were also specifically expressed in branch cells
395 (Vandepoele et al., 2002). Other branch-cell-specific genes included *AURI* and *AUR2*, both

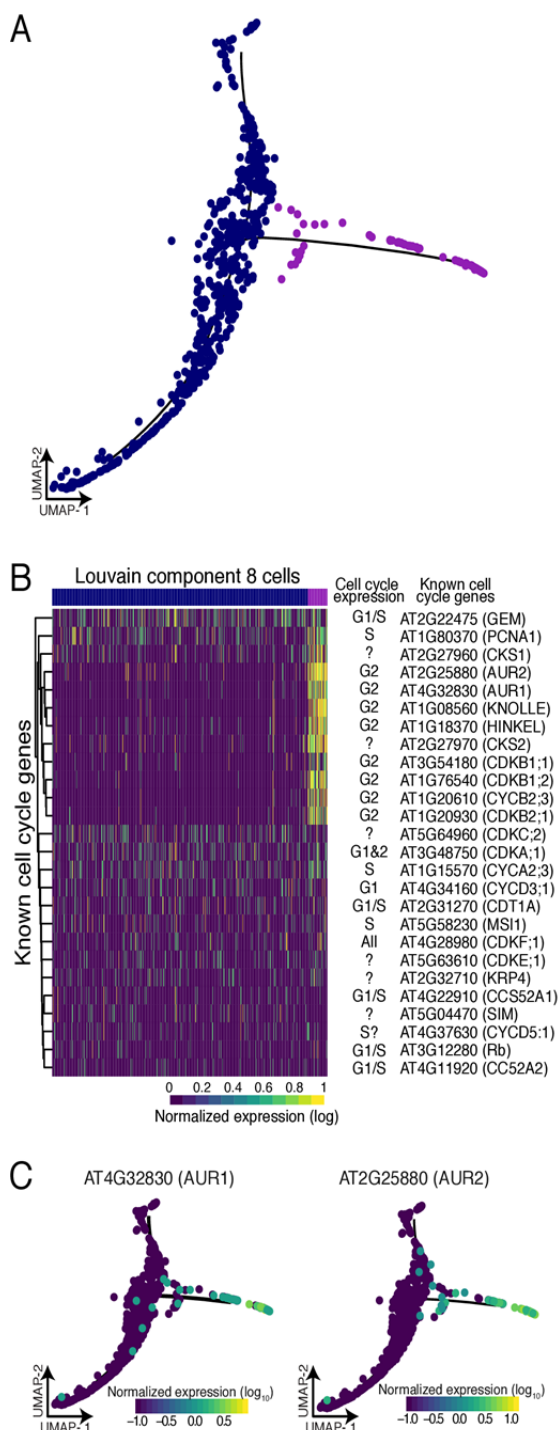


Figure 6. Branch analysis reveals actively dividing cells. (A) The 70 cells that resided in the branch of Louvain component 8 (purple) show significant branch-specific expression of genes enriched for cell cycle function. (B) Comparison of all known cell cycle genes with expression in at least 5% of cells in Louvain component 8. Known cell cycle expression is denoted for each gene, if unknown '?'. (C) Two kinases, AUR1 and AUR2, were specifically expressed in branch cells. These genes are involved in cell plate formation and lateral root formation.

396 involved in lateral root formation and cell plate formation (Figure 6C, Van Damme et al., 2011).

397 Louvain component 9 also showed a strong, but short branching point. We did not find any
398 biological processes enriched in genes expressed specifically in this short branch; however, one
399 gene whose expression is known to be affected by protoplasting was specifically expressed in
400 these cells, perhaps reflecting that cells within this branch were more stressed by our
401 experimental procedure (data not shown).

402

403 **Heat-shocked root cells show subtle expression differences among cell types**

404 A major question in studying plant responses to abiotic stress, such as heat or drought, is the
405 extent to which such responses are non-uniform across cell types. Canonically, the heat stress
406 response is characterized by rapid and massive up-regulation of a few loci, mostly encoding heat
407 shock proteins, with dramatic down-regulation of most other loci, in part because of altered
408 mRNA splicing and transport (Saavedra et al., 1996; Yost and Lindquist, 1986, 1988). In plants,
409 a set of 63 genes, most encoding heat shock proteins, show extreme chromatin accessibility at
410 both promoter and gene body upon heat stress, consistent with their high expression (Sullivan et
411 al., 2014). In mammals and insects, not all cells are competent to exhibit the hallmarks of the
412 heat shock response (Dura, 1981; Morange et al., 1984); specifically, cells in early embryonic
413 development fail to induce heat shock protein expression upon stress.

414

415 We explored whether all cells within developing roots were capable of exhibiting a typical heat
416 shock response. To do so, we applied a standard heat stress (45 min, 38°C) to eight-day-old
417 seedlings, harvested their roots along with roots from age- and time-matched control seedlings,
418 and generated protoplasts for single-cell RNA-seq of both samples. For the control sample, we
419 captured 1076 cells, assaying expression for a median 4,079 genes per cell and a total of 22, 971
420 genes; 82.7% of reads mapped to the TAIR10 genome assembly. The results for these control
421 cells were similar to those described earlier with regard to captured cell types, proportion of cell
422 types (*e.g.* 28.8% vs. 34% annotated hair cells and 9.7% vs. 7.2% endodermis cells), and
423 correlation of gene expression ($R^2 = 0.86$ for the 21,107 genes captured in both experiments). For
424 the heat shock sample, we captured 1,009 cells, assaying expression for a median 4,384 genes
425 per cell and a total of 21,237 genes; 79.8% of reads mapped to the TAIR10 genome assembly.

426

427 Due to global gene expression changes upon heat shock, we could not simply assign cell and
428 tissue types as before for heat-shocked cells. The overwhelming impact of heat shock was also
429 apparent when comparing the first and second highest cell type and developmental Spearman's
430 rank correlations for control cells and heat-shocked cells. Upon heat shock, many cells,
431 especially those with non-hair, phloem and columella as their highest rank, commonly showed as
432 their second highest rank a different cell type instead of another developmental time point of the
433 same cell type as observed in control cells (**Supplemental Figure 11A**). Unsurprisingly, the
434 drastic changes in gene expression led to cells being embedded in UMAP space primarily as a
435 function of treatment, making direct comparisons of treatment effects on any one cell type
436 impossible (**Supplemental Figure 11B**). To enable such comparisons, we used a mutual nearest
437 neighbor to embed cells conditioned on treatment in UMAP space (Haghverdi et al., 2018). The
438 mutual nearest neighbor method was originally developed to account for batch effects by
439 identifying the most similar cells between each batch and applying a correction to enable proper
440 alignment of data sets. Here, we employ this technique to overcome the lack of marker
441 expression in our heat-shock treated cells and match them to their untreated counterpart based on
442 overall transcriptome similarity (**Figure 7A**). This procedure yielded corresponding clusters in
443 control and heat-shocked cells, albeit with varying cell numbers for most (**Supplemental Figure**
444 **11C, Supplemental Table 2**).

445
446 In response to stress, organisms are thought to upregulate stress genes and to specifically
447 downregulate genes involved in growth and development to optimize resource allocation. In
448 response to heat stress, this presumed 'dichotomy' in gene expression is mirrored by the rapid
449 localization of RNA polymerase II to the heat shock gene loci and its depletion elsewhere in the
450 genome (Teves and Henikoff, 2011). Our data provide strong evidence of this regulatory trade-
451 off at the level of individual cells. Using hair cells (Louvain component 2) as an example, we
452 found that hair-cell-specific genes are overwhelmingly repressed and that heat shock genes are
453 upregulated, often dramatically so (**Figure 7B-D**). Indeed, *HSP101*, the most highly expressed
454 and chromatin-accessible gene upon heat shock in previous studies (Sullivan et al., 2014), was
455 strongly expressed across all clusters while expression of the hair marker gene *COBL9* decreased
456 dramatically upon stress (**Figure 7C, D**).

457

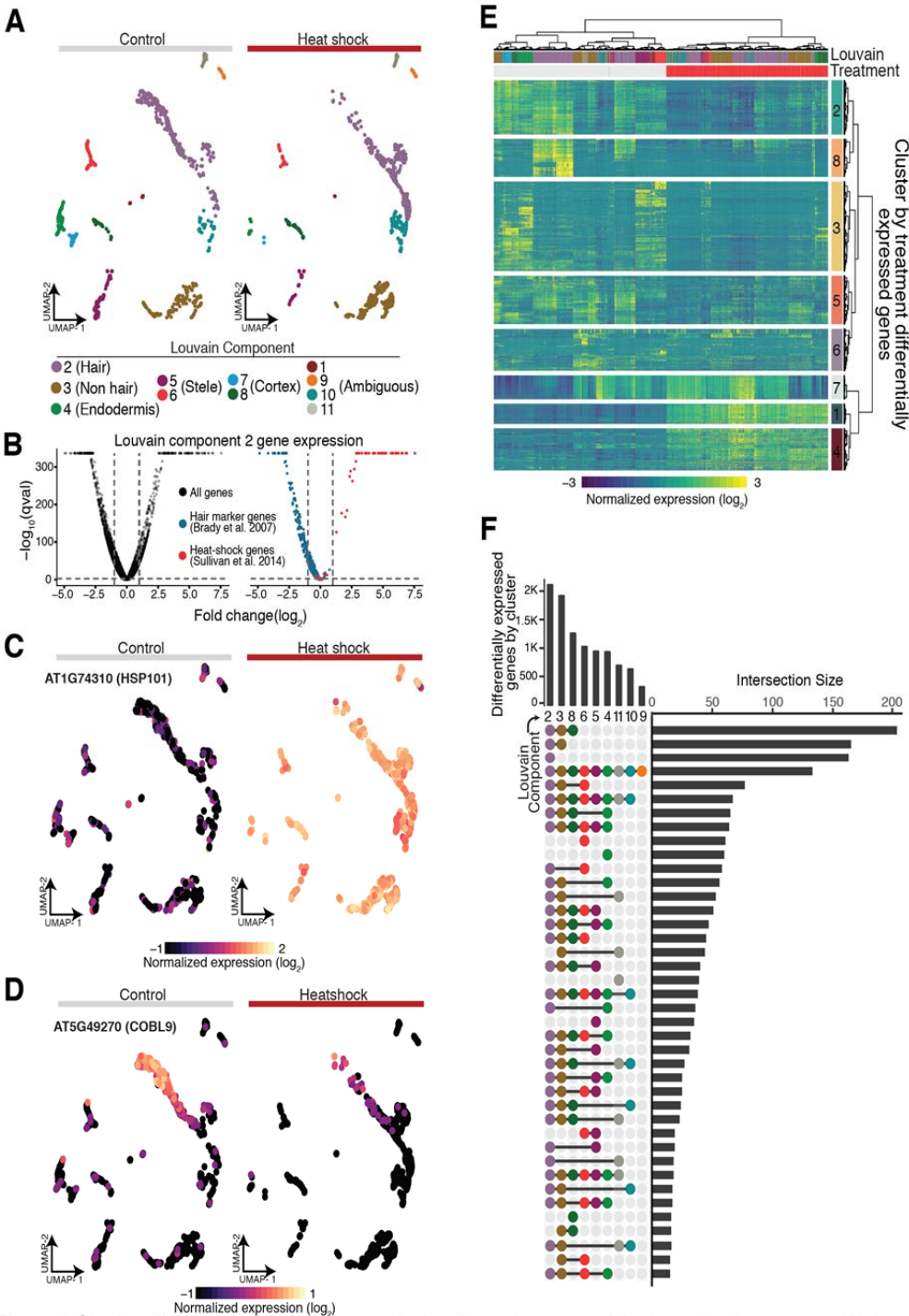


Figure 7. Single cell RNA-seq highlights canonical and novel aspects of the heat shock response. (A) A nearest neighbor approach aligns control and heat-shocked cells in a UMAP embedding to allow for concomitant cluster/cell type assignment. (B) Volcano plots of average gene expression change upon heat shock within Louvain component 2 for all genes (black), known hair marker genes (blue) and heat-shock signature genes (red). (C) HSP101, a signature heat shock gene, shows dramatic increase of expression in all cell types upon heat shock. (D) COBL9, a well-studied hair marker gene, is strongly repressed upon heat shock. (E) Heat map of differentially expressed genes upon heat shock (top red bar; control, top gray bar), hierarchically clustered by both cells and genes (FDR < 0.1% and absolute value of the \log_2 fold change > 1). (F) Upset plot (Lex et al., 2014) of the number of differentially expressed genes as a function of heat shock for each Louvain cluster in our UMAP embedding (bars on top) along with the number of the intersect of differentially expressed genes between Louvain clusters (bars on the right). A surprising number of differentially expressed genes were specific to certain clusters (single dot in vertical row of dots).

458 Having established comparable clusters, we next identified genes that were differentially

459 expressed as a function of treatment and cluster identity, excluding those with less than 15 cells
460 in either control or heat shock conditions. This analysis identified 8,526 genes (FDR < 0.1%)
461 whose expression was altered by heat shock treatment in one or more clusters; of these, 2,627
462 genes were up- or downregulated at least 2-fold (**Figure 7E, Supplementary Data Set 5**, FDR
463 < 0.1% and absolute value of log₂ fold change > 1). As for hair cells (**Figure 7B**), cell-type
464 marker genes for all clusters were enriched among the downregulated genes upon heat shock. To
465 identify cluster-specific differences in the response to heat shock, we compared gene expression
466 of cells within individual clusters to the rest of the cells across treatments. We observed the
467 largest number of cluster-specific gene expression changes in hair, non-hair and cortex cells
468 (**Figure 7F**). As these cell types are the three outermost cell layers of the root, they may be
469 exposed more directly to the heat shock and respond more quickly. Genes differentially
470 expressed in hair cells (Louvain component 2) upon heat shock were enriched for ribosome
471 associated genes and RNA methylation. Stele cells (Louvain component 6) showed differential
472 expression of genes involved in cell wall organization and biogenesis, and endodermis cells
473 (Louvain component 4) showed differential expression of genes involved in response to external,
474 chemical and stress stimuli as well as nitrate and anion transport (**Figure 7F**).

475
476 The expression of heat shock proteins protects cells from heat shock and aids their recovery
477 (Parsell et al., 1993; Parsell and Lindquist, 1993; Queitsch et al., 2000). We were interested in
478 whether we could detect cluster- and cell-type-specific differences in the canonical heat shock
479 response. In principle, such differences could be exploited to alter heat shock protein expression
480 in a cell-type-specific manner to boost plant heat and drought tolerance without pleiotropically
481 decreasing whole-organism fitness. To address such possible differences, we focused on genes
482 that from bulk analyses have differential expression upon heat shock (1783 genes) or reside near
483 regulatory regions that change in accessibility upon heat shock (1730 genes) (Alexandre et al.,
484 2018; Sullivan et al., 2014). Although these gene sets overlap (942 genes), they contain
485 complementary information, as changes in accessibility do not necessarily translate into altered
486 expression, and vice versa (Alexandre et al., 2018). In our single-cell expression analysis, we
487 identified 752 of 1783 heat-responsive genes as differentially expressed upon heat shock, and
488 564 of 1730 genes near dynamic regulatory regions as differentially expressed. We hierarchically
489 clustered control and heat shock-treated single-cell transcriptomes for both gene sets

490 **(Supplemental Figure 12A, C)**, resulting in several gene clusters with distinct expression
491 patterns. Overall, cellular responses were dominated by the canonical heat-shock response, as
492 visualized in cluster 4 **(Supplemental Figure 12A)** and cluster 2 **(Supplemental Figure 12C)**.
493 The 63 genes showing extreme accessibility and high expression upon heat shock (Sullivan et al.,
494 2014) are largely contained in these two clusters **(Supplemental Figure 12A, cluster 4, 49 of 63;**
495 **Supplemental Figure 12C, cluster 2, 42 of 63)**.

496
497 Our analysis also revealed subtle but significant differences among some tissue types
498 **(Supplemental Figure 12A, B, e.g. clusters 3 and 8, Supplemental Figure 12C, D, e.g. clusters**
499 **5 and 7, Supplemental Data Set 6)**. Although most of these gene clusters were not enriched for
500 specific annotations, cluster 8 genes were associated with rRNA metabolic processes (p-
501 value=0.048) and cluster 5 genes **(Supplemental Figure 12A, B)** were enriched for transport
502 genes (p-value=0.045). These results demonstrate both the promise and the challenges inherent
503 in comparing single-cell data across different conditions and treatments.

504
505

506 **DISCUSSION**

507 Here, we use *A. thaliana* roots to establish both experimental and analytic procedures for single-
508 cell RNA-seq in plants. Using Monocle 3, we could assign over 3000 cells to expected cell and
509 tissue types with high confidence. In particular, cortex, endodermis and hair cells were easily
510 identified. However, distinguishing other cell types was challenging. For example, non-hair and
511 columella cells had high similarity in their expression profiles, consistent with their correlation in
512 bulk expression data (Brady et al., 2007; Cartwright et al., 2009). Similarly, it was difficult to
513 designate cells in Louvain component 8 as early non-hair cells, as these cells showed
514 overlapping expression signatures for early non-hair cells, lateral root caps, and epidermis cells
515 before differentiation to hair and non-hair cells. These Louvain component 8 cells were difficult
516 to distinguish further with the sparse expression data typical for single cell analysis, however we
517 postulate that in fact the branch of component 8 may actually be the root of the trajectory and are
518 cells dividing out of the epidermis/root cap precursor and cells either become root cap cells or
519 epidermis.

520
521 We also could not initially split stele tissue into individual cell types, likely because the
522 difficulty of digesting the cell walls of the tightly packed vascular bundle resulted in fewer cells
523 than expected (Brady et al., 2007; Cartwright et al., 2009). However, analyzing stele cells
524 separately yielded 6 sub-clusters, which correspond to known vasculature cell types. Our
525 approach to annotate these sub-clusters exemplifies the ad hoc nature of current single-cell
526 genomics studies, which require all available sources of information to be exploited to interpret
527 the genomic data. Neither Spearman rank correlations with sorted bulk RNA-seq data nor
528 microarray expression data yielded obvious cluster identities. However, mean expression values
529 of genes known to be expressed in vasculature cell types allowed us to assign the stele sub-
530 clusters.

531
532 We identified hundreds of novel genes with cell-type-specific and tissue-type-specific
533 expression, which may allow the generation of new marker lines for detailed genetic analyses.
534 These genes, together with cluster-specific enriched transcription factor motifs and their
535 corresponding transcription factors, are candidates for driving differentiation and cell-type
536 identity. Similarly, the developmental trajectories we identified highlight the potential of single

537 cell transcriptomics to advance a high resolution view of plant development. These trajectories
538 can be detected without the use of spatial information because plants have a continuous body
539 plan with new cells continuously arising while older cells persist. Additionally, while this study
540 allowed us to infer transcription factor motifs and candidate transcription factors, future analyses
541 with greater numbers of cells than assayed here may include combinatorial expression of
542 multiple transcription factor family members.

543

544 We explored the relationships of endoreduplication, transcriptional rates, and
545 differentiation to find that transcriptional rates, measured as mRNA velocity, increase with
546 increasing ploidy. However, this transcriptional increase appears to be limited to genes
547 specifically expressed in hair cells, as overall levels of RNA decreased over pseudotime. These
548 observations are consistent with hair cells becoming more specialized and moving towards a
549 terminally differentiated state over time. However, this phenomenon of increasing specialization
550 was not as apparent in other cell types. This difference may be due to biological causes, such as
551 the higher rates of endoreduplication in hair cells, or to technical causes, such as the better
552 clustering and trajectory of hair cells compared to the other cell types assayed.

553

554 By allowing trajectories with side branches, we discovered that branch points can mark
555 developmental decisions. In Louvain component 8, the small but distinct cell-cycle enriched
556 branch may mark lateral root primordia cells differentiating into epidermal cells or
557 epidermal/lateral root precursor cells. Cells within this branch express many cell cycle genes,
558 among them members of the *CDKB* family that govern the G2 to M transition. Moreover, these
559 cells specifically express the *AUR1* and *AUR2* genes, which function in cell plate formation;
560 plants with mutations in these genes lack lateral roots (Van Damme et al., 2011). Although
561 expression of cell cycle genes may persist in non-dividing cells because of their roles in
562 endoreduplication, *AUR1* and *AUR2* expression (and cell plate formation) should not persist,
563 consistent with our speculation that the cells within this branch are actively dividing cells in the
564 G2 to M transition (Gutierrez, 2009).

565

566 We explored the *A. thaliana* heat shock response with single-cell RNA-seq because not
567 all cells and tissues are equally competent to respond to stress. By identifying plant cell types

568 that most strongly respond to abiotic stresses such as heat, drought, and nutrient starvation,
569 ultimately we may be able to genetically manipulate relevant cell types to generate stress-tolerant
570 crops without pleiotropically affecting plant fitness and yield. Although all heat-shocked cells
571 showed gene expression changes typical of the canonical heat shock genes, we detected subtle
572 but highly significant expression differences among cells and tissue types for other genes. Thus,
573 single-cell transcriptomics across stress conditions holds potential for future crop breeding and
574 genetic engineering. However, such analyses require much larger numbers of cells than currently
575 accessible by droplet-based methods. Moreover, such analyses should focus on treatments that
576 are less overwhelmed by a strong canonical signal to increase resolution in detecting cell-type-
577 specific differences.

578
579 In this study, we relied on the extensive and detailed expression data for bulk *A. thaliana*
580 cell and tissue types to establish the validity of our approaches. The overwhelming
581 correspondence of our findings with these and other data derived from traditional molecular
582 genetics provides confidence that less well-characterized *A. thaliana* tissues and other plants,
583 including crops, will be amenable to these approaches. Thus, continued progress on single-cell
584 RNA-seq experiments should have a major impact on the analysis of plant development and
585 environmental response.

586
587

589 METHODS

590 **Plant Material and Growth Conditions.** *Arabidopsis thaliana* Col-0 seedlings were grown
591 vertically at 22°C, on 1xMS + 1% sucrose plates covered with one layer of filter paper. Seven or
592 eight days-old seedlings (LD, 16h light/8h dark, ~100 $\mu\text{mol m}^2 \text{ s}$) were collected around ZT3,
593 and the roots/shoots excised with a sharp razor blade. For the heat-shock, seedling plates were
594 transferred from 22°C to 38°C for 45 min (Convicon TC-26, light ~100 $\mu\text{mol m}^2 \text{ s}$), and the roots
595 harvested immediately after.

596

597 **Protoplast Isolation.** Protoplast isolation was done as previously described (Bargmann and
598 Birnbaum, 2010), with slight modifications. Briefly, 1 g of whole-roots was incubated in 10 ml
599 of protoplasting solution for 1.5 h at 75 rpm. After passing through a 40 μm strainer, protoplasts
600 were centrifuged at 500 g for 5 min and washed once in protoplasting solution without enzymes.
601 Final suspension volume was adjusted to a density of 500 – 1,000 cells/ μl . Protoplasts were
602 placed on ice until further processing.

603

604 Single-cell RNA-seq protocol

605 Single-cell RNA-seq was performed on fresh *Arabidopsis* root protoplast using the 10X scRNA-
606 seq platform, the Chromium Single Cell Gene Expression Solution (10X Genomics).

607

608 Data Analysis

609 *Estimating gene expression in individual cells*

610 Single-cell RNA-seq reads were sequenced and then mapped to the TAIR10 *Arabidopsis* genome
611 using Cellranger (version 2.1.0) ([https://support.10xgenomics.com/single-cell-gene-](https://support.10xgenomics.com/single-cell-gene-expression/software/pipelines/latest/what-is-cell-ranger)
612 [expression/software/pipelines/latest/what-is-cell-ranger](https://support.10xgenomics.com/single-cell-gene-expression/software/pipelines/latest/what-is-cell-ranger)). Cellranger produces a matrix of UMI
613 counts where each row is a gene and each column represents a cell. The ARAPORT gene
614 annotation was used. For the heat shock analysis, reads from a control sample and reads from
615 heat-shocked sample were aggregated using “cellranger aggr” to normalize libraries to
616 equivalent number of mean reads per cell across libraries.

617

618 *Running Monocle 3: Dimensionality Reduction, and Cell Clustering* The output of the cellranger
619 pipeline was parsed into R (version 3.5.0) using the cellranger R kit (version 2.0.0) and

620 converted into a CellDataSet (cds) for further analysis using Monocle 3 alpha (version 2.99.1)
621 (<http://cole-trapnell-lab.github.io/monocle-release/monocle3/>). All Monocle 3 analysis was
622 performed on a High Performance Computing cluster using 128GB of RAM spread across 8
623 cores. The lower detection limit for the cds was set at 0.5, and the expression family used set to
624 `negbinomial.size()`.

625

626 We visualized cell clusters and trajectories using the standard Monocle workflow. Monocle
627 internally handles all normalization needed for dimensionality reduction, visualization, and
628 differential expression via “size factors” that control for variability in library construction
629 efficiency across cells. After estimating the library size factors for each cell (via
630 `estimateSizeFactors`), and estimating the dispersion in expression for each gene (via
631 `estimateDispersions`) in the dataset, the top 1500 genes in terms of dispersion, *i.e.* 1500 genes
632 with the most expression variability in our dataset, were selected to order the cells into clusters.
633 The expression values of these 1500 genes for each cell were log-transformed and projected onto
634 the first 25 principal components via Monocle’s data pre-processing function (`preprocessCDS`).
635 Then, these lower-dimensional coordinates were used to initialize a nonlinear manifold learning
636 algorithm implemented in Monocle 3 called Uniform Manifold Approximation and Projection, or
637 UMAP (via `reduceDimension`) (McInnes and Healy, 2018). This allows us to visualize the data
638 unto two or three dimensions. Specifically, we projected onto 2 components using the cosine
639 distance metric, setting the parameters “`n_neighbors`” to 50, and “`min_dist`” to 0.1.

640

641 The Louvain method was used to detect cell clusters in our two dimensional representation of the
642 dataset (`partitionCells`); this resulted in 11 cell clusters, or Louvain components. Cells were then
643 clustered into “super” groups using a method derived from “approximate graph abstraction”
644 (Wolf et al., 2018) and for each super group, a cell trajectory was drawn atop the projection
645 using Monocle’s reversed graph embedding algorithm, which is derived from “SimplePPT”
646 (`learnGraph`) (Mao et al., 2015). This yielded 6 cell trajectories.

647

648 To further analyze the clusters we annotated as stele, Clusters 3, 4, and 7 were reclustered
649 together and were reanalyzed using Monocle 3 as previously described except the parameter

650 “min_dist” was changed to 0.05 when the reduceDimension function was called. This revealed 6
651 additional sub clusters.

652
653 To further analyze the cluster we annotated as cortex, Cluster 10 was reclustered and reanalyzed
654 using Monocle 3 as previously described except the parameters “n_neighbors” was reduced to
655 25. This did not reveal any sub clusters, but a trajectory was generated.

656
657 *Estimating doublets*

658 **Single-Cell Remover of Doublets** (Scrublet) was used to predict doublets in our scRNA-seq data
659 (Available at: <https://github.com/AllonKleinLab/scrublet>). Using Python 3.5, Scrublet was ran
660 using default settings as described by the example tutorial which is available as a python
661 notebook (Available at:
662 https://github.com/AllonKleinLab/scrublet/blob/master/examples/scrublet_basics.ipynb). The
663 only significant change was that expected double rate was set to 0.1, in the tutorial it is 0.06.

664
665 *Identifying Cell Types*

666 In order to categorize the cells into cell types and to apply developmental information, a
667 deconvolved root expression map was downloaded from AREX LITE: The Arabidopsis Gene
668 Expression Database (<http://www.arexdb.org/data/decondatamatrix.zip>). Using this data matrix,
669 the Spearman’s rank correlation was calculated between each cell in our dataset and each cell
670 type and longitudinal annotation in the data matrix (3121 x 128 Spearman’s rank correlations
671 total). Specifically, we looked at the correlation of 1229 highly variable genes in our dataset.
672 These 1229 genes represents the overlap between our 1500 highly variable genes and genes in
673 the root expression map data matrix. Cells in our dataset were assigned a cell type and a
674 developmental label based on the annotation with which each cell had the highest correlation.
675 (*i.e.* if a cell correlated highest with endodermis cells in longitudinal zone 11, then it would be
676 called as endodermis_11).

677
678 In addition to using the Spearman’s rank correlation to assign cells their cell type, a set of known
679 marker genes derived from GFP marker lines of the Arabidopsis root were used to identify cell
680 types based on the high gene expression of these marker genes. These genes were obtained from

681 (Brady et al., 2007; Cartwright et al., 2009). Specifically Supplemental Table 2 (Cartwright et
682 al., 2009) was used. For the analysis comparing bulk RNA and pseudo bulk scRNA-seq data, the
683 bulk data was obtained from Li et al. 2016 (Li et al., 2016); specifically, we used Table S5 from
684 this study. Isoforms of each gene were averaged in order to be comparable to the pseudo bulk
685 data. Lastly, using this same bulk RNA-seq data, the Pearson correlation was calculated between
686 each cell in our dataset and each GFP marker line. Cells in our dataset were assigned to a GFP
687 marker line based on the GFP marker line with which each cell had the highest correlation.

688

689 *Running Monocle 3: Identifying High Specificity Genes*

690 In order to identify differentially expressed genes between cell clusters the Moran's I test was
691 performed on our UMAP (principalGraphTest), with the projection being broken up into 25 x 25
692 spatial units. Then marker genes were identified for each cluster, and each annotated grouping of
693 clusters using a Moran's I threshold of 0.1 and a qval threshold of 0.05. In order for a gene to be
694 considered highly specific, it must have had a specificity rating of above 0.7.

695

696 *Transcription factor motif analysis*

697 Highly specific genes were identified for each cell cluster, and their promoters were analyzed for
698 presence of transcription factor motifs. Promoters were defined as 500 base pairs upstream of the
699 start site of each gene. Instances of each motif were identified using (Grant et al., 2011) at a p-
700 value cutoff of 1e-5 for each match. The input position weight matrices for each motif were
701 enumerated in a previous study of binding preferences for nearly all Arabidopsis transcription
702 factors (O'Malley et al., 2016). Motif frequencies in genes specific to each cell cluster were
703 compared to a background set of motif frequencies across all promoters in the Arabidopsis
704 genome to determine a log2 enrichment score. TF family genes were pulled from the gene family
705 page of TAIR10 (<https://www.arabidopsis.org/browse/genefamily/index.jsp>).

706

707 *Running Monocle 3: Assigning Pseudotime*

708 Pseudotime analysis requires the selection of a cell as an "origin" for the pseudotime trajectory.
709 Origin assignment was based on the Spearman's rank assignments for each cell. The following
710 cells were used as origins for their respective cell type trajectories: cortex_2, hair_2,

711 endodermis_2, nonHair_3. The `get_correct_root_state()` function was used to assign the root of a
712 trajectory, and the `orderCells()` function was used to assign cells a pseudotime value.

713

714 *Calculating total mRNA*

715 After pseudotime analysis was performed on a cell cluster, cells were binned together such that
716 each bin contained a similar number of cells and each bin represented cells from similar
717 pseudotimes. The median total mRNA and the standard deviation of the total mRNA of each bin
718 was then calculated.

719

720

721 *Calculating significance with the Permutation Test*

722 The permutation test was used to calculate the significance of the observed trends that the total
723 mRNA of hair marker genes and hair specific genes increased as pseudotime increased in hair
724 cells. To do this, 10000 random samplings of 441 genes (the number of hair marker genes), and
725 201 genes (the number of hair specific genes) were taken respectively. Next, the median total
726 mRNA was calculated across pseudotime for each random sampling and the slope of this data
727 was calculated using a generalized linear model. The observed slope of the marker genes and the
728 hair specific genes was compared to the distribution of slopes generated by 10000 random
729 samplings. No random sampling of genes had a slope that was higher than the observed slopes
730 generated by the hair marker genes or the hair specific genes. The significance, or the p-value, of
731 the trend seen in the hair marker genes and the hair specific genes can then be calculated simply
732 as the proportion of sampled permutations that have a slope that is equal to or greater than slope
733 generated by our genes of interest. This gives us a p-value of 1/10001 or roughly 1×10^{-4} .

734

735 *Analyzing Expression Differences Between Branches of Louvain Component 8 (Early Non-Hair)*

736 To identify genes responsible for the branching in the pseudotime trajectory of Louvain
737 component 8 (early non-hair), the principal graph test was used to identify genes with expression
738 specific to the side branch vs. the main branch. Genes were considered specific if it had a
739 specificity value above 0.8. Genes were removed from the analysis if they did not have
740 expression in at least 10% of the cells considered and a mean expression greater than 0.25.

741

742 *Calculating RNA velocity*

743 We used the Velocity R and Python packages (version 0.6 and 0.17, respectively) to estimate
744 RNA velocity for root hair cells (La Manno et al., 2018). Matrices of spliced and unspliced RNA
745 counts were generated from Cellranger outputs using velocity.py CLI and "run10x" defaults. We
746 followed the velocity.py and velocity.R manuals (<http://velocity.org/>) and used spliced (emat)
747 and unspliced (nmat) matrices to estimate RNA velocity. With predefined cell type annotations,
748 we performed gene filtering with the parameter "min.max.cluster.average" set to 0.2 and 0.05 for
749 "emat" and "nmat", respectively. RNA velocity using the selected 996 genes was estimated with
750 the defaults to the function gene.relative.velocity.estimate() except parameters "kCells" and
751 "fit.quantile" which were set to 5 and 0.05, respectively. Velocity measurements for each cell
752 were calculated as the difference between "\$projected" and "\$current" (with $\Delta T = 1$) results
753 from the estimated velocity output.

754

755 *Analysis of heat shock data*

756 For each pair of cell types and for each gene cluster, we used a generalized linear model to
757 determine the significance of an interaction between the effects of cell type and heat treatment on
758 the normalized expression level of genes in that cluster. Then, to identify differentially expressed
759 genes specific for every Louvain cluster we subsetted cells from every cluster that contained 15
760 or more cells in both control and treated conditions, estimated dispersions for each subset and
761 tested for differential gene expression identified using the differentialGeneTest function in
762 Monocle specifying a full model of Treatment cluster and a residual model of 1. FDR values per
763 gene were then obtained across all tests using the Benjamini-Hochberg method. The overlap of
764 differentially expressed genes as a function of heatshock treatment between clusters was
765 visualized using an UpsetR plot. Briefly, a binary matrix of differentially expressed genes by
766 cluster was generated where gene-cluster combinations were set to 1 (significant) or 0 (not
767 significant). This matrix was then passed to the upset function from the UpsetR R package
768 specifying 9 sets and ordering by frequency. To identify whether clusters contained subtle
769 differences in the expression of previously identified heat shock responsive genes we tested for
770 differential gene expression across all cells and clusters and identified the intersect between
771 differentially expressed genes obtained from single cell profiles and previously identified
772 dynamic changes in DHS linked genes and bulk differentially expressed genes upon heat shock.

773 Differentially expressed genes as a function of heat-shock treatment for all cells in unison where
774 identified using the differentialGeneTest function in Monocle specifying a full model of
775 Treatment*UMAP cluster and a residual model of UMAP cluster. Hierarchical clustering of
776 these DHS linked and bulk differentially expressed gene sets across control and heat-shock
777 treated cells was performed using the pheatmap function in the pheatmap R package (version
778 1.0.10) specifying ward.D2 as the clustering method. Genes with similar dynamics across
779 treatment and cell types were recovered using the cutree function from the stats package in R
780 specifying $k = 8$ for both DHS linked genes and bulk differentially expressed genes. To generate
781 signatures from these 8 groups of clustered genes we log normalized expression values using a
782 pseudocount of 1 and for each cell calculated the mean normalized expression value across genes
783 that belong to one of the 8 gene cluster.

784

785 **Data Availability**

786 All sequencing data can be found on GEO at:

787 <https://www.ncbi.nlm.nih.gov/geo/query/acc.cgi?acc=GSE121619>

788 **Supplemental Data**

789 **Supplemental Figure 1:** General tissue and data features

790 **Supplemental Figure 2:** Pearson correlation to sorted RNA-seq samples

791 **Supplemental Figure 3:** Marker gene expression in cell type clusters

792 **Supplemental Figure 4:** Examples of tissue-specific gene expression

793 **Supplemental Figure 5:** Transcription factor family expression patterns

794 **Supplemental Figure 6:** Spearman's rank correlation for each cell's development and tissue-
795 type

796 **Supplemental Figure 7:** Changes in transcription across hair development

797 **Supplemental Figure 8:** Developmental trajectory of endodermal cells

798 **Supplemental Figure 9:** Total RNA in cortex across pseudotime

799 **Supplemental Figure 10:** Developmental expression of individual transcription factors

800 **Supplemental Figure 11:** Heat-shock clustering and expression profiling

801 **Supplemental Figure 12:** Conditional expression in genes with dynamic chromatin accessibility
802 during heat-shock

803 **Supplemental Table 1:** Bulk RNA-seq comparisons to single cell RNA-seq

804 **Supplemental Table 2:** Number of cells in the control vs. heatshock analysis

805 **Supplemental Data Set 1:** List of Ordering/ High Dispersion Genes

806 **Supplemental Data Set 2:** Correlation with Bulk Expression Data

807 **Supplemental Data Set 3:** Marker Genes

808 **Supplemental Data Set 4:** Novel High Specificity Genes

809 **Supplemental Data Set 5:** Cluster Specific Heat shock Differentially Expressed Genes

810 **Supplemental Data Set 6:** Generalized Linear Model pairwise test of significance between

811 cortex, hair, and non-hair cells

812

813 **ACKNOWLEDGEMENTS**

814 We thank members of the Trapnell Lab for input and discussion. This work was supported by

815 NSF MCB-1516701 to CQ and NSF RESEARCH-PGR 1748843 to CQ and SF. KJB was

816 supported by the University of Washington NIH Big Data for Genomics and Neuroscience

817 Training Grant (T32LM012419). NIH grant U54DK107979 to CT; NIH grant DP2HD088158,

818 RC2DK114777 and R01HL118342 to CT; and the Paul G. Allen Frontiers Group to CT.

819

820

Parsed Citations

Alexandre, C.M., Urton, J.R., Jean-Baptiste, K., Huddleston, J., Dorrity, M.W., Cuperus, J.T., Sullivan, A.M., Bemm, F., Jolic, D., Arsovski, A.A., et al. (2018). Complex Relationships between Chromatin Accessibility, Sequence Divergence, and Gene Expression in *Arabidopsis thaliana*. *Mol Biol Evol* 35, 837-854.

Pubmed: [Author and Title](#)

Google Scholar: [Author Only](#) [Title Only](#) [Author and Title](#)

Bargmann, B.O.R. and Birnbaum, K.D. (2010). Fluorescence Activated Cell Sorting of Plant Protoplasts. *J. Vis. Exp.*

Pubmed: [Author and Title](#)

Google Scholar: [Author Only](#) [Title Only](#) [Author and Title](#)

Bennett, T., van den Toorn, A., Sanchez-Perez, G.F., Campilho, A., Willemsen, V., Snel, B., and Scheres, B. (2010). SOMBRERO, BEARSKIN1, and BEARSKIN2 regulate root cap maturation in *Arabidopsis*. *Plant Cell* 22, 640-654.

Pubmed: [Author and Title](#)

Google Scholar: [Author Only](#) [Title Only](#) [Author and Title](#)

Bhosale, R., Boudolf, V., Cuevas, F., Lu, R., Eekhout, T., Hu, Z., van Isterdael, G., Lambert, G., Xu, F., Nowack, M.K., et al. (2018). A spatiotemporal DNA endoploidy map of the *Arabidopsis* root reveals roles for the endocycle in root development and stress adaptation. *Plant Cell*.

Pubmed: [Author and Title](#)

Google Scholar: [Author Only](#) [Title Only](#) [Author and Title](#)

Birnbaum, K., Shasha, D.E., Wang, J.Y., Jung, J.W., Lambert, G.M., Galbraith, D.W., and Benfey, P.N. (2003). A gene expression map of the *Arabidopsis* root. *Science* 302, 1956-1960.

Pubmed: [Author and Title](#)

Google Scholar: [Author Only](#) [Title Only](#) [Author and Title](#)

Blonde, V.D., Guillaume, J.-L., Lambiotte, R., and Lefebvre, E. (2008). Fast unfolding of communities in large networks. *Journal of Statistical Mechanics: Theory and Experiment* 2008.

Pubmed: [Author and Title](#)

Google Scholar: [Author Only](#) [Title Only](#) [Author and Title](#)

Bourdon, M., Pirrello, J., Cheniclet, C., Coriton, O., Bourge, M., Brown, S., Moise, A., Peypelut, M., Rouyere, V., Renaudin, J.P., et al. (2012). Evidence for karyoplasmic homeostasis during endoreduplication and a ploidy-dependent increase in gene transcription during tomato fruit growth. *Development* 139, 3817-3826.

Pubmed: [Author and Title](#)

Google Scholar: [Author Only](#) [Title Only](#) [Author and Title](#)

Brady, S.M., Orlando, D.A., Lee, J.Y., Wang, J.Y., Koch, J., Dinneny, J.R., Mace, D., Ohler, U., and Benfey, P.N. (2007). A high-resolution root spatiotemporal map reveals dominant expression patterns. *Science* 318, 801-806.

Pubmed: [Author and Title](#)

Google Scholar: [Author Only](#) [Title Only](#) [Author and Title](#)

Brennecke, P., Anders, S., Kim, J.K., Kołodziejczyk, A.A., Zhang, X., Proserpio, V., Baying, B., Benes, V., Teichmann, S.A., Marioni, J.C., and Heisler, M.G. (2013). Accounting for technical noise in single-cell RNA-seq experiments. *Nat. Methods* 10: 1093-1095.

Pubmed: [Author and Title](#)

Google Scholar: [Author Only](#) [Title Only](#) [Author and Title](#)

Cao, J., Packer, J.S., Ramani, V., Cusanovich, D.A., Huynh, C., Daza, R., Qiu, X., Lee, C., Furlan, S.N., Steemers, F.J., et al. (2017). Comprehensive single-cell transcriptional profiling of a multicellular organism. *Science* 357, 661-667.

Pubmed: [Author and Title](#)

Google Scholar: [Author Only](#) [Title Only](#) [Author and Title](#)

Cartwright, D.A., Brady, S.M., Orlando, D.A., Sturmfels, B., and Benfey, P.N. (2009). Reconstructing spatiotemporal gene expression data from partial observations. *Bioinformatics* 25, 2581-2587.

Pubmed: [Author and Title](#)

Google Scholar: [Author Only](#) [Title Only](#) [Author and Title](#)

Van Damme, D., De Rybel, B., Gudesblat, G., Demidov, D., Grunewald, W., De Smet, I., Houben, A., Beeckman, T., and Russinova, E. (2011). *Arabidopsis* α Aurora kinases function in formative cell division plane orientation. *Plant Cell* 23: 4013-24.

Pubmed: [Author and Title](#)

Google Scholar: [Author Only](#) [Title Only](#) [Author and Title](#)

Dura, J.M. (1981). Stage dependent synthesis of heat shock induced proteins in early embryos of *Drosophila melanogaster*. *Mol Gen Genet* 184, 381-385.

Pubmed: [Author and Title](#)

Google Scholar: [Author Only](#) [Title Only](#) [Author and Title](#)

Efroni, I., Ip, P.-L., Nawy, T., Mello, A., and Birnbaum, K.D. (2015). Quantification of cell identity from single-cell gene expression profiles. *Genome Biol.* 16: 9.

Pubmed: [Author and Title](#)

Google Scholar: [Author Only](#) [Title Only](#) [Author and Title](#)

Efroni, I., Mello, A., Nawy, T., Ip, P.-L., Rahni, R., DelRose, N., Powers, A., Satija, R., and Birnbaum, K.D. (2016). Root Regeneration Triggers an Embryo-like Sequence Guided by Hormonal Interactions. *Cell* 165: 1721–1733.

Pubmed: [Author and Title](#)

Google Scholar: [Author Only](#) [Title Only](#) [Author and Title](#)

Grant, C.E., Bailey, T.L., and Noble, W.S. (2011). FIMO: scanning for occurrences of a given motif. *Bioinformatics* 27, 1017-1018.

Pubmed: [Author and Title](#)

Google Scholar: [Author Only](#) [Title Only](#) [Author and Title](#)

Gutierrez, C. (2009). The Arabidopsis cell division cycle. *Arab. B.* 7: e0120.

Pubmed: [Author and Title](#)

Google Scholar: [Author Only](#) [Title Only](#) [Author and Title](#)

Haghverdi, L., Lun, A.T.L., Morgan, M.D., and Marioni, J.C. (2018). Batch effects in single-cell RNA-sequencing data are corrected by matching mutual nearest neighbors. *Nat Biotechnol* 36, 421-427.

Pubmed: [Author and Title](#)

Google Scholar: [Author Only](#) [Title Only](#) [Author and Title](#)

Irish, V.F. (1991). Cell lineage in plant development. *Curr Opin Cell Biol* 3, 983-987.

Pubmed: [Author and Title](#)

Google Scholar: [Author Only](#) [Title Only](#) [Author and Title](#)

Katayama, H., Iwamoto, K., Kariya, Y., Asakawa, T., Kan, T., Fukuda, H., and Ohashi-Ito, K. (2015). A Negative Feedback Loop Controlling bHLH Complexes Is Involved in Vascular Cell Division and Differentiation in the Root Apical Meristem. *Curr Biol* 25, 3144-3150.

Pubmed: [Author and Title](#)

Google Scholar: [Author Only](#) [Title Only](#) [Author and Title](#)

Kieffer, M., Master, V., Waites, R., and Davies, B. (2011). TCP14 and TCP15 affect internode length and leaf shape in Arabidopsis. *Plant J* 68, 147-158.

Pubmed: [Author and Title](#)

Google Scholar: [Author Only](#) [Title Only](#) [Author and Title](#)

La Manno, G. et al. (2018). RNA velocity of single cells. *Nature* 560: 494–498.

Pubmed: [Author and Title](#)

Google Scholar: [Author Only](#) [Title Only](#) [Author and Title](#)

Lachowiec, J., Lemus, T., Thomas, J.H., Murphy, P.J., Nemhauser, J.L., and Queitsch, C. (2013). The protein chaperone HSP90 can facilitate the divergence of gene duplicates. *Genetics* 193, 1269-1277.

Pubmed: [Author and Title](#)

Google Scholar: [Author Only](#) [Title Only](#) [Author and Title](#)

Lachowiec, J., Mason, G.A., Schultz, K., and Queitsch, C. (2016). Redundancy, feedback, and robustness in the Arabidopsis thaliana BZR/BEH gene family. *bioRxiv*.

Pubmed: [Author and Title](#)

Google Scholar: [Author Only](#) [Title Only](#) [Author and Title](#)

Lachowiec, J., Mason, G.A., Schultz, K., and Queitsch, C. (2018). Redundancy, feedback, and robustness in the Arabidopsis thaliana BZR/BEH gene family. *bioRxiv* 053447; doi: <https://doi.org/10.1101/053447>.

Pubmed: [Author and Title](#)

Google Scholar: [Author Only](#) [Title Only](#) [Author and Title](#)

Lan, X., and Pritchard, J.K. (2016). Coregulation of tandem duplicate genes slows evolution of subfunctionalization in mammals. *Science* 352, 1009-1013.

Pubmed: [Author and Title](#)

Google Scholar: [Author Only](#) [Title Only](#) [Author and Title](#)

Lee, C., Teng, Q., Zhong, R., and Ye, Z.H. (2012). Arabidopsis GUX proteins are glucuronyltransferases responsible for the addition of glucuronic acid side chains onto xylan. *Plant Cell Physiol* 53, 1204-1216.

Pubmed: [Author and Title](#)

Google Scholar: [Author Only](#) [Title Only](#) [Author and Title](#)

Lex, A., Gehlenborg, N., Strobel, H., Vuillemot, R., and Pfister, H. (2014). UpSet: Visualization of Intersecting Sets. *IEEE Trans. Vis. Comput. Graph.* 20: 1983–92.

Pubmed: [Author and Title](#)

Google Scholar: [Author Only](#) [Title Only](#) [Author and Title](#)

Li, S., Yamada, M., Han, X., Ohler, U., and Benfey, P.N. (2016). High-Resolution Expression Map of the Arabidopsis Root Reveals Alternative Splicing and lincRNA Regulation. *Dev Cell* 39, 508-522.

Pubmed: [Author and Title](#)

Google Scholar: [Author Only](#) [Title Only](#) [Author and Title](#)

Lucero, L.E., Uberti-Manassero, N.G., Arce, A.L., Colombatti, F., Alemanno, S.G., and Gonzalez, D.H. (2015). TCP15 modulates cytokinin and auxin responses during gynoecium development in Arabidopsis. *Plant J* 84, 267-282.

Pubmed: [Author and Title](#)

Google Scholar: [Author Only](#) [Title Only](#) [Author and Title](#)

Mao, Q., Yang, L., Wang, L., Goodison, S., and Sun, Y. (2015). SimplePPT: A Simple Principal Tree Algorithm Proceedings of the 2015 SIAM International Conference on Data Mining, 792–800.

Pubmed: [Author and Title](#)

Google Scholar: [Author Only](#) [Title Only](#) [Author and Title](#)

McInnes, L., and Healy, J. (2018). UMAP: Uniform Manifold Approximation and Projection for Dimension Reduction. ArXiv e-prints 180203426.

Pubmed: [Author and Title](#)

Google Scholar: [Author Only](#) [Title Only](#) [Author and Title](#)

Morange, M., Diu, A., Bensaude, O., and Babinet, C. (1984). Altered expression of heat shock proteins in embryonal carcinoma and mouse early embryonic cells. Mol Cell Biol 4, 730-735.

Pubmed: [Author and Title](#)

Google Scholar: [Author Only](#) [Title Only](#) [Author and Title](#)

Mortimer, J.C., Miles, G.P., Brown, D.M., Zhang, Z., Segura, M.P., Weimar, T., Yu, X., Seffen, K.A., Stephens, E., Turner, S.R., et al. (2010). Absence of branches from xylan in Arabidopsis gux mutants reveals potential for simplification of lignocellulosic biomass. Proc Natl Acad Sci U S A 107, 17409-17414.

Pubmed: [Author and Title](#)

Google Scholar: [Author Only](#) [Title Only](#) [Author and Title](#)

O'Malley, R.C., Huang, S.C., Song, L., Lewsey, M.G., Bartlett, A., Nery, J.R., Galli, M., Gallavotti, A., and Ecker, J.R. (2016). Cistrome and Epicistrome Features Shape the Regulatory DNA Landscape. Cell 165, 1280-1292.

Pubmed: [Author and Title](#)

Google Scholar: [Author Only](#) [Title Only](#) [Author and Title](#)

Ohashi-Ito, K., Saegusa, M., Iwamoto, K., Oda, Y., Katayama, H., Kojima, M., Sakakibara, H., and Fukuda, H. (2014). AbHLH complex activates vascular cell division via cytokinin action in root apical meristem. Curr Biol 24, 2053-2058.

Pubmed: [Author and Title](#)

Google Scholar: [Author Only](#) [Title Only](#) [Author and Title](#)

Packer, J., and Trapnell, C. (2018). Single-Cell Multi-omics: An Engine for New Quantitative Models of Gene Regulation. Trends Genet 34, 653-665.

Pubmed: [Author and Title](#)

Google Scholar: [Author Only](#) [Title Only](#) [Author and Title](#)

Parsell, D.A and Lindquist, S. (1993). The Function of Heat-Shock Proteins in Stress Tolerance: Degradation and Reactivation of Damaged Proteins. Annu. Rev. Genet. 27: 437–496.

Pubmed: [Author and Title](#)

Google Scholar: [Author Only](#) [Title Only](#) [Author and Title](#)

Parsell, D.A, Taulien, J., and Lindquist, S. (1993). The role of heat-shock proteins in thermotolerance. Philos. Trans. R. Soc. London. Ser. B Biol. Sci. 339: 279–286.

Pubmed: [Author and Title](#)

Google Scholar: [Author Only](#) [Title Only](#) [Author and Title](#)

Peng, Y., Chen, L., Lu, Y., Wu, Y., Dumenil, J., Zhu, Z., Bevan, M.W., and Li, Y. (2015). The ubiquitin receptors DA1, DAR1, and DAR2 redundantly regulate endoreduplication by modulating the stability of TCP14/15 in Arabidopsis. Plant Cell 27, 649-662.

Pubmed: [Author and Title](#)

Google Scholar: [Author Only](#) [Title Only](#) [Author and Title](#)

Petricka, J.J., Winter, C.M., and Benfey, P.N. (2012). Control of Arabidopsis root development. Annu Rev Plant Biol 63, 563-590.

Pubmed: [Author and Title](#)

Google Scholar: [Author Only](#) [Title Only](#) [Author and Title](#)

Plant Illustrations Shoot illustrations.

Qiu, X., Hill, A., Packer, J., Lin, D., Ma, Y.A., and Trapnell, C. (2017a). Single-cell mRNA quantification and differential analysis with Census. Nat Methods 14, 309-315.

Pubmed: [Author and Title](#)

Google Scholar: [Author Only](#) [Title Only](#) [Author and Title](#)

Qiu, X., Mao, Q., Tang, Y., Wang, L., Chawla, R., Pliner, H.A., and Trapnell, C. (2017b). Reversed graph embedding resolves complex single-cell trajectories. Nat Methods 14, 979-982.

Pubmed: [Author and Title](#)

Google Scholar: [Author Only](#) [Title Only](#) [Author and Title](#)

Queitsch, C., Hong, S.W., Vierling, E., and Lindquist, S. (2000). Heat shock protein 101 plays a crucial role in thermotolerance in Arabidopsis. Plant Cell 12: 479–492.

Pubmed: [Author and Title](#)

Google Scholar: [Author Only](#) [Title Only](#) [Author and Title](#)

Resentini, F., Felipo-Benavent, A., Colombo, L., Blazquez, M.A., Alabadi, D., and Masiero, S. (2015). TCP14 and TCP15 mediate the promotion of seed germination by gibberellins in Arabidopsis thaliana. Mol Plant 8, 482-485.

Pubmed: [Author and Title](#)

Google Scholar: [Author Only Title Only Author and Title](#)

Riechmann, J.L., Heard, J., Martin, G., Reuber, L., Jiang, C., Keddie, J., Adam, L., Pineda, O., Ratcliffe, O.J., Samaha, R.R., et al. (2000). Arabidopsis transcription factors: genome-wide comparative analysis among eukaryotes. *Science* 290, 2105-2110.

Pubmed: [Author and Title](#)

Google Scholar: [Author Only Title Only Author and Title](#)

Rogers, E.D., and Benfey, P.N. (2015). Regulation of plant root system architecture: implications for crop advancement. *Curr Opin Biotechnol* 32, 93-98.

Pubmed: [Author and Title](#)

Google Scholar: [Author Only Title Only Author and Title](#)

Russell, A.B., Trapnell, C., and Bloom, J.D. (2018). Extreme heterogeneity of influenza virus infection in single cells. *Elife* 7.

Pubmed: [Author and Title](#)

Google Scholar: [Author Only Title Only Author and Title](#)

Saavedra, C., Tung, K.S., Amberg, D.C., Hopper, A.K., and Cole, C.N. (1996). Regulation of mRNA export in response to stress in *Saccharomyces cerevisiae*. *Genes Dev* 10, 1608-1620.

Pubmed: [Author and Title](#)

Google Scholar: [Author Only Title Only Author and Title](#)

Sullivan, A.M., Arsovski, A.A., Lempe, J., Bubb, K.L., Weirauch, M.T., Sabo, P.J., Sandstrom, R., Thurman, R.E., Neph, S., Reynolds, A.P., et al. (2014). Mapping and dynamics of regulatory DNA and transcription factor networks in *A. thaliana*. *Cell Rep* 8, 2015-2030.

Pubmed: [Author and Title](#)

Google Scholar: [Author Only Title Only Author and Title](#)

Tan, T.T., Endo, H., Sano, R., Kurata, T., Yamaguchi, M., Ohtani, M., and Demura, T. (2018). Transcription Factors VND1-VND3 Contribute to Cotyledon Xylem Vessel Formation. *Plant Physiol* 176, 773-789.

Pubmed: [Author and Title](#)

Google Scholar: [Author Only Title Only Author and Title](#)

Tatematsu, K., Nakabayashi, K., Kamiya, Y., and Nambara, E. (2008). Transcription factor AtTCP14 regulates embryonic growth potential during seed germination in *Arabidopsis thaliana*. *Plant J* 53, 42-52.

Pubmed: [Author and Title](#)

Google Scholar: [Author Only Title Only Author and Title](#)

Teves, S.S. and Henikoff, S. (2011). Heat shock reduces stalled RNA polymerase II and nucleosome turnover genome-wide. *Genes Dev.* 25: 2387-2397.

Pubmed: [Author and Title](#)

Google Scholar: [Author Only Title Only Author and Title](#)

Trapnell, C. (2015). Defining cell types and states with single-cell genomics. *Genome Res* 25, 1491-1498.

Pubmed: [Author and Title](#)

Google Scholar: [Author Only Title Only Author and Title](#)

Trapnell, C., Cacchiarelli, D., Grimsby, J., Pokharel, P., Li, S., Morse, M., Lennon, N.J., Livak, K.J., Mikkelsen, T.S., and Rinn, J.L. (2014). The dynamics and regulators of cell fate decisions are revealed by pseudotemporal ordering of single cells. *Nat Biotechnol* 32, 381-386.

Pubmed: [Author and Title](#)

Google Scholar: [Author Only Title Only Author and Title](#)

Winter, D., Vinegar, B., Nahal, H., Ammar, R., Wilson, G.V., and Provart, N.J. (2007). An "Electronic Fluorescent Pictograph" browser for exploring and analyzing large-scale biological data sets. *PLoS One* 2, e718.

Pubmed: [Author and Title](#)

Google Scholar: [Author Only Title Only Author and Title](#)

Wolf, F.A., Hamey, F., Plass, M., Solana, J., Dahlin, J.S., Gottgens, B., Rajewsky, N., Simon, L., and Theis, F.J. (2018). Graph abstraction reconciles clustering with trajectory inference through a topology preserving map of single cells. *bioRxiv*, doi: <https://doi.org/10.1101/208819>

Pubmed: [Author and Title](#)

Google Scholar: [Author Only Title Only Author and Title](#)

Wolock, S.L., Lopez, R., and Klein, A.M. (2018). Scrublet: computational identification of cell doublets in single-cell transcriptomic data. *bioRxiv*: 357368.

Pubmed: [Author and Title](#)

Google Scholar: [Author Only Title Only Author and Title](#)

Vandepoele, K., Raes, J., De Veylder, L., Rouzé, P., Rombauts, S., and Inzé, D. (2002). Genome-wide analysis of core cell cycle genes in *Arabidopsis*. *Plant Cell* 14: 903-16.

Pubmed: [Author and Title](#)

Google Scholar: [Author Only Title Only Author and Title](#)

Yost, H.J., and Lindquist, S. (1986). RNA splicing is interrupted by heat shock and is rescued by heat shock protein synthesis. *Cell* 45, 185-193.

Pubmed: [Author and Title](#)

Google Scholar: [Author Only](#) [Title Only](#) [Author and Title](#)

Yost, H.J., and Lindquist, S. (1988). Translation of unspliced transcripts after heat shock. Science 242, 1544-1548.

Pubmed: [Author and Title](#)

Google Scholar: [Author Only](#) [Title Only](#) [Author and Title](#)

Zhu, D., Wu, Z., Cao, G., Li, J., Wei, J., Tsuge, T., Gu, H., Aoyama, T., and Qu, L.J. (2014). TRANSLUCENT GREEN, an ERF family transcription factor, controls water balance in Arabidopsis by activating the expression of aquaporin genes. Mol Plant 7, 601-615.

Pubmed: [Author and Title](#)

Google Scholar: [Author Only](#) [Title Only](#) [Author and Title](#)